Constraint-Based Analysis of Parallel Kinematic Articulated Wrist Mechanisms

by

Revanth Damerla

A dissertation submitted in partial fulfillment
of the requirements for the degree of
Master of Science in Engineering
(Mechanical Engineering)
in the University of Michigan
2020

Thesis Committee:

Associate Professor Shorya Awtar

Revanth Damerla

damerla@umich.edu

ORCID iD: 0000-0003-2472-9894

TABLE OF CONTENTS

LIST OF TABLES

LIST OF FIGURES

ABSTRACT

This thesis presents a systematic constraint-based analysis of the performance attributes of eight parallel kinematic articulated wrist mechanisms from the existing literature. These performance attributes include the number, nature (i.e. pure rotation, or translation, or a combination), and location of a mechanism's Degrees of Freedom (DoFs) in the nominal and displaced configurations, range of operation along these DoFs, load transmission capability along these DoFs, and load bearing capability along the constraint directions. This systematic analysis reveals performance tradeoffs between these performance attributes for a given mechanism, as well as design tradeoffs across these mechanisms. This analysis also helps inform the suitability of a given mechanism for specific applications.

CHAPTER 1

Introduction and Background

Articulated wrist mechanisms offer at least two rotations (commonly designated as pitch and yaw) and are used in a wide range of applications that require dexterous manipulation, remote access, or orientation adjustment. These applications include minimally invasive surgery [1–10], measuring displacements of a Conclusion human interface for control [10–12], industrial operations such as robotic welding and spay-painting [13,14], handling of hazardous material [13,14], varying the orientation of a camera or other sensor in commercial [7,15,16] or aerospace [17,18] applications, varying the pointing angle of a fire extinguisher [19], and various robotic operations [20–24], to name a few. This wide range of applications has led to many unique articulated wrist mechanisms with various performance attributes, which determine the suitability of a mechanism for a given application.

These performance attributes include the Degrees of Freedom (DoFs) and Degrees of Constraint (DoCs) of an End Effector of a mechanism with respect to its Base (Fig. 1). DoFs are the independent directions of motion that the End Effector can undergo while DoCs are the independent directions that the End Effector is constrained to not move along. DoFs are geometrically represented by *freedom lines* that capture pure rotation, pure translation, or a combination (i.e. screw). Similarly, DoCs are represented by *constraint lines* that capture translational constraint, rotational constraint, or a combination (i.e. wrench). The freedom lines of a mechanism together form its freedom space, and similarly all the constraint lines of a

mechanism form its constraint space. The freedom and constraint spaces of a mechanism define how it moves and transmits loads.

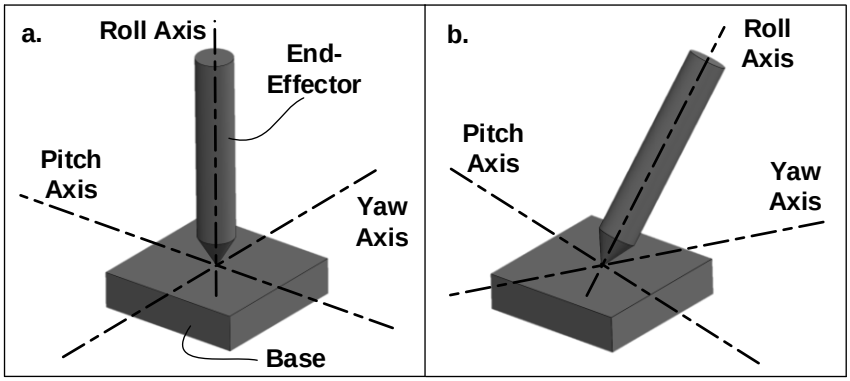

Fig. 1 Generic Articulated Wrist Mechanism: a. Nominal configuration, b. Displaced configuration

Freedom lines and constraint lines follow certain basic rules of geometry: DoFs add in series, DoCs add in parallel, and they are complementary to each other. The latter, known as the Rule of Complementary Patterns [25], states that if there are *n* independent constraint lines, then there will be 6-*n* independent freedom lines, each of which will intersect every constraint line. Thus, the freedom and constraint spaces are complementary. This rule can be used to identify freedom spaces from constraint spaces and vice versa. Screw theory provides a mathematical representation of the same concepts, which is beneficial when the constraint and freedom spaces are challenging to visualize and analyze using straightforward geometric arguments [26–33]. The Freedom and Constraint Topology (FACT) framework builds upon these geometric and mathematical principles to provide a comprehensive catalog of all possible constraint and freedom spaces [33–35]. In this thesis, we will make use of these geometric and mathematical tools to analyze freedom and constraint spaces.

An articulated wrist mechanism offers at least two rotational DoFs (pitch and yaw) between an End Effector and Base, as shown in Fig. 1. Depending on the application, the mechanism can also have additional DoFs such as roll rotation or translation along the central

axis. In an ideal scenario, at least in the nominal configuration, the two rotational DoFs (pitch and yaw) are pure rotations about their respective axes (Fig. 1a). In this nominal configuration, it is helpful to construct a central axis that is orthogonal to both the pitch and yaw axes, passes through the point of intersection of these two axes, and is affixed to the End Effector. In a displaced configuration (Fig. 1b), the central axis retains its location with respect to (w.r.t.) the End Effector. Several performance attributes that impact the performance and suitability of an articulated wrist mechanism for a given application are compiled below to capture the scope of investigation in this thesis:

1. *Number of DoFs of the End Effector w.r.t. the Base in the nominal and displaced configurations.* The mechanism may exhibit redundant constraint lines in the nominal configuration that become non-redundant in the displaced configuration, or vice versa, resulting in an unexpected or undesired change in the number of DoF as the mechanism displaces. This can impact the range of motion and utility of the mechanism.
2. *Location of the DoFs in the nominal and displaced configurations.* Change in location can mean that, upon displacement of the mechanism from its nominal configuration, the pitch and yaw rotational DoFs no longer remain in the same plane, or orthogonal, or intersect at the same point, or intersect at all, or a combination of these. This implies that the center of rotation of the End Effector w.r.t. the Base may drift, the axes of rotation may drift, and that the End Effector tip may not trace a perfect hemisphere.
3. *Nature of the DoFs in the nominal and displaced configurations.* Change in nature can mean that the two DoFs (pitch and yaw) no longer remain purely rotational, and instead have a coupled translational component that is kinematically tied to the rotations (i.e. screw motion). This also implies that the End Effector will not trace a perfect

hemisphere.

4. The articulated wrist mechanism is intended to bear loads along its DoC directions, and therefore *load bearing capability (or equivalently stiffness)* in these directions is critical. This is impacted by the mechanism's kinematics (e.g. transmission angles) and construction (e.g. joint or link stiffness) of the mechanism, both of which can vary from nominal to displaced configurations.
5. If the articulated wrist mechanism is used in an active application where actuation loads are transmitted from inputs on the mechanism (e.g. yaw input and pitch input) to the End Effector output, then *load transmission capability (or equivalently transmission stiffness)* becomes critical. This is also impacted by the kinematics and construction of the mechanism and can vary from nominal to displaced configurations.

As noted above, these performance attributes typically deviate from nominal behavior with increasing displacement of the mechanism, thereby potentially creating a performance tradeoff between these attributes and range of motion. Range of motion is also impacted by practical considerations such as the sizes of links and joints in the mechanism and collisions between them.

An articulated wrist mechanism can be either serial kinematic or parallel kinematic in its architecture. Parallel kinematic mechanisms allow ground mounted actuators, making them preferable in active applications. They can also be more compact and lightweight, resulting in faster speeds. However, their design and evaluation (qualitative as well as quantitative) is more complex [15,25–40]. Because of these reasons along with their wide applicability, we focus on parallel kinematic articulated wrist mechanisms in this thesis. We identify eight mechanisms from the literature (see Fig. 2) and present a systematic and comprehensive constraint-based

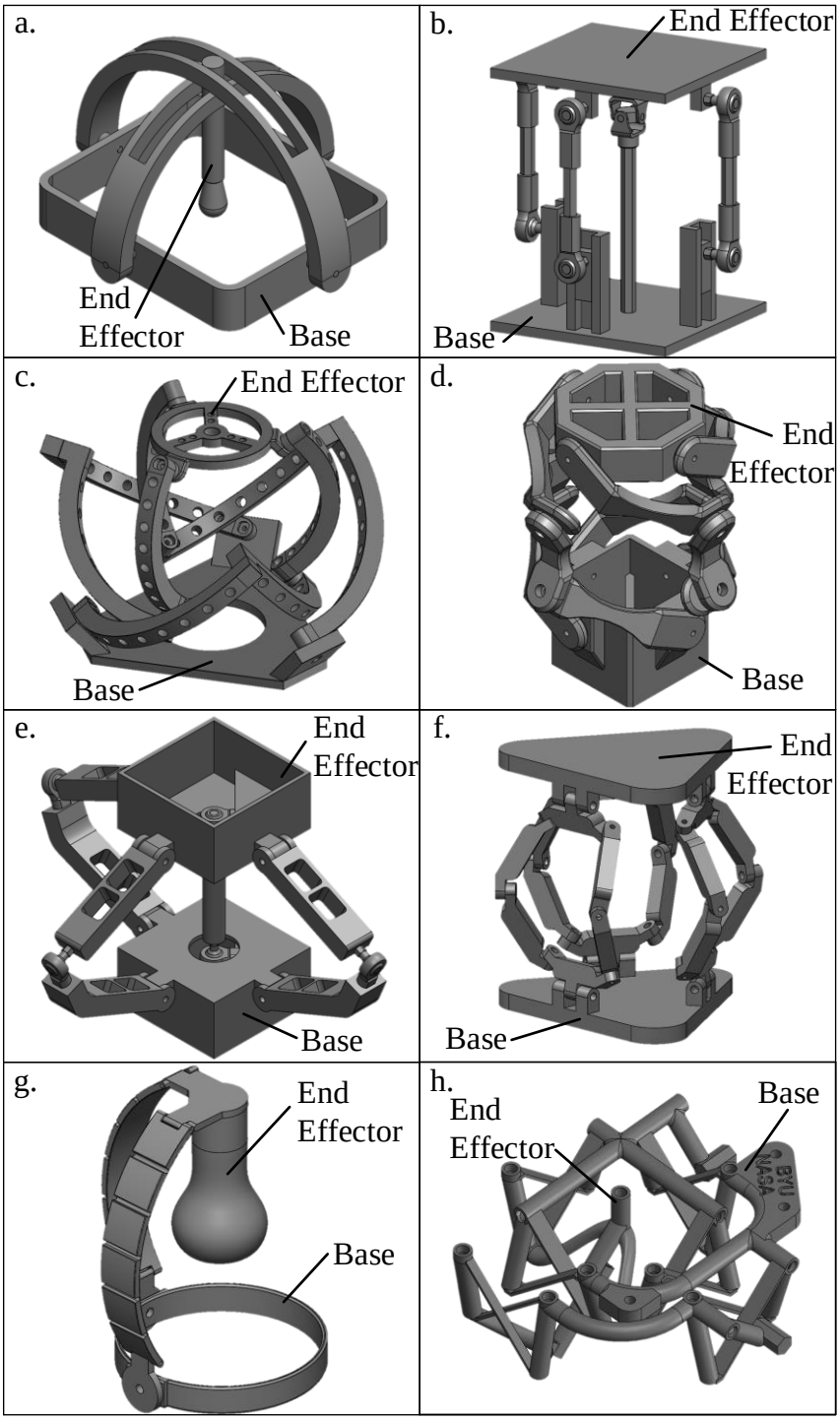

Fig. 2 Parallel Kinematic Articulated Wrist Mechanisms: a. Dual Arch, b. Tip-Tilt Plate, c. Agile Eye, d. OmniWrist III, e. OmniWrist V, f. 3-Spherical Kinematic Chain Parallel Mechanism, g. FlexDex, h. BYU Space Pointing Mechanism

analysis of their performance attributes, with the goal of generating insights into performance tradeoffs (within a given mechanism) and design tradeoffs (between the various mechanisms).

These mechanisms were chosen primarily for their diversity in architecture, performance, and applications. As a result, they provide a representative set of the design tradeoffs that can be expected within parallel kinematic articulated wrist mechanisms. The Dual Arch [6,10–12] (Fig. 2a), Tip-Tilt Plate [23] (Fig. 2b), and Agile Eye [15] (Fig. 2c) mechanisms are composed entirely of rigid joints and links. These mechanisms offer ideal pitch and yaw DoFs, meaning they remain pure rotations and retain their nominal intersection point even after displacement. The next three mechanisms are the OmniWrist III [19,41] (Fig. 2d), the OmniWrist V [42] (Fig. 2e), and the 3-Spherical Kinematic Chain Parallel Mechanism [1,38] (Fig. 2f), which are also entirely composed of rigid links and joints. However, their pitch and yaw rotational DoFs do not remain purely rotational upon displacement. Next, the FlexDex® mechanism [9,10] (Fig. 2g) has some links and joints that are rigid and some that are compliant. Under the assumption of finite compliance along certain DoCs, this mechanism is also shown to offer yaw and pitch DoFs. The BYU Space Pointing mechanism [17] (Fig. 2h) is a monolithic mechanism composed of rigid links and compliant joints. The compliance enables pitch and yaw DoFs, which may not retain their nominal behavior.

1.1 Screw Theory for the Constraint-Based Analysis of Parallel Kinematic Mechanisms

Screw theory is an analytical tool that can be used to define the motion of an object. It is useful within a Constraint-Based Analysis because it can mathematically identify the DoFs or DoCs of a mechanism. Screw theory can therefore be seen as the mathematical analog for the geometrically driven method laid out in [25]. It is especially helpful in cases when the

mechanism's geometry is very complicated or when screw DoFs or wrench DoCs are present. Several resources can provide additional details on screw theory beyond the scope of this section as well as worked out examples [26–33].

A screw describes the motion of a rigid body in free space. Physically the body is represented as connected to a screw with pitch and a specific orientation and location. It is defined mathematically as a 6×1 vector as shown in Eq. 1 [27,30,31,33].

$$\$ = \begin{bmatrix} \vec{\omega} \\ \vec{v} \end{bmatrix} = \begin{bmatrix} \vec{\omega} \\ \vec{r} \times \vec{\omega} + p\vec{\omega} \end{bmatrix} \tag{1}$$

The upper 3×1 vector $\vec{\omega}$ describes the angular velocity of the body and the lower 3×1 vector $\vec{v}$ describes its linear velocity. $\vec{r}$ is the vector from the origin to any point along the screw and the scalar p is the pitch of the screw, as shown in Fig. 3. A screw can also represent a freedom line where $\vec{\omega}$ describes the axis of rotation and $\vec{v}$ describes the translation, location, and pitch. Thus, the screw $[1\ 0\ 0\ 0\ 0\ 0]^T$ represents a pure rotational freedom line passing through the origin; $[0\ 0\ 0\ 1\ 0\ 0]^T$ represents a pure translational DoF; $[1\ 0\ 0\ 1\ 0\ 0]^T$ represents a screw freedom line with a pitch of 1 passing through the origin.

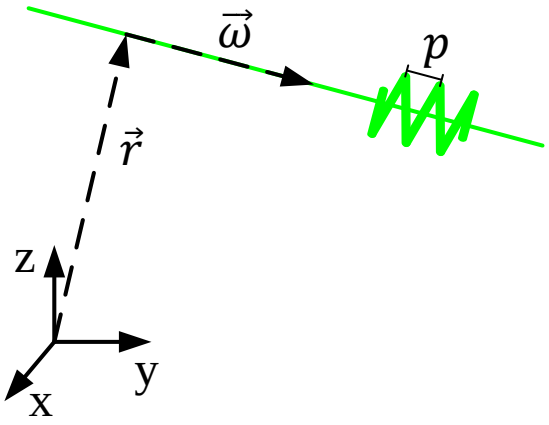

Fig. 3 Example of a Screw Freedom Line, Adapted from [33]

Similarly, a wrench describes a load applied to a body. It is also defined as a 6x1 vector

as shown in Eq. 2 [31,33].

$$W = \begin{bmatrix} \vec{F} \\ \vec{\tau} \end{bmatrix} = \begin{bmatrix} \vec{F} \\ \vec{r} \times \vec{F} + q\vec{F} \end{bmatrix} \quad (2)$$

Here, $\vec{F}$ describes the applied force, $\vec{\tau}$ describes the applied moment, $\vec{r}$ is the vector from the origin to any point along $\vec{F}$, and the scalar q is a coupling term between force and moment. A wrench can represent a constraint line where $\vec{F}$ describes the direction of its linear components and $\vec{\tau}$ describes the rotational components, location, and coupling. For example, the wrench $[1\ 0\ 0\ 0\ 0\ 0]^T$ represents a pure translational constraint line passing through the origin; $[0\ 0\ 0\ 1\ 0\ 0]^T$ represents a pure rotational DoC; $[1\ 0\ 0\ 1\ 0\ 0]^T$ represents a wrench constraint line with a coupling of 1 passing through the origin.

With the mathematical definitions of freedom and constraint lines in place, it is possible to complete the Constraint-Based Analysis of a parallel kinematic mechanism. This typically begins with finding the freedom space of each serial kinematic chain. In a serial kinematic chain, joints with specific DOFs connect rigid bodies together. The End Effector is connected to the end of this chain and therefore has a combination of all of the DoFs provided by the joints in the chain. Each DoF can be described by a single screw and a freedom matrix can be generated that is a combination of each screw. For a serial chain with *k* joints providing *l* DOFs, a $6\times l$ freedom matrix SL can be created where each DoF is described by a screw, S_i, as shown in Eq. 3.

$$SL = [S_1 \quad S_2 \quad \ldots \quad S_l] \quad (3)$$

The value of l can be greater than six and the number of redundant freedom lines will not impact the calculations.

The constraints of the End Effector intuitively describe the directions of motion that an End Effector cannot undergo. This corresponds to applied loads that do not produce any motion

and therefore do not produce a power output. This would lead to the relationship shown in Eq. 4, where $\vec{\tau}$ and $\vec{F}$ are the applied moment and force, respectively and $\vec{\omega}$ and $\vec{v}$ are the angular and linear velocity of the End Effector, respectively.

$$\vec{\tau} \cdot \vec{\omega} + \vec{F} \cdot \vec{v} = 0 \tag{4}$$

Eq. 4 can be expressed as Eq. 5 [27–31], where the matrix Δ is a 6×6 matrix that ensures that the linear and rotational terms from Eq. 4 are combined; I and 0 are identity and zero matrices, respectively.

$$SL\Delta CL = \begin{bmatrix} S_1 & S_2 & \dots & S_l \end{bmatrix}^T \begin{bmatrix} 0_{3\times3} & I_{3\times3} \\ I_{3\times3} & 0_{3\times3} \end{bmatrix} \begin{bmatrix} C_1 & C_2 & \dots & C_m \end{bmatrix} = 0_{l\times m} \tag{5}$$

This is known as the Reciprocal Product and is a mathematical relation equivalent to the Rule of Complementary Patterns. It provides a method to find the corresponding constraint space for a known freedom space and vice versa. Eq. 5 can be viewed as a null space problem of the form $AX = 0$ where A is $SL\Delta$ and X corresponds to the matrix CL. Thus, the corresponding constraint space consists of constraints that span the null space of the freedom space. SL and CL can also be reversed so that the corresponding freedom space can be found from the constraint space. To understand the Reciprocal Product intuitively, consider that six independent freedom and constraint lines are needed to adequately describe the mobility of any rigid body. Since these lines are independent, these freedom and constraint lines together span the 6-dimensional space consisting of the three independent translations and three independent rotations of a rigid body. In Eq. 5, CL (i.e. the set DoCs) represents the set of motions not spanned by SL (i.e. the set of DoFs) within this 6-dimensional space.

Once the constraints of the mechanism's n serial kinematic chains are found, they can be added together to form the mechanism constraint space as shown in Eq. 6, where CL_i corresponds to the constraint matrix of the ith serial kinematic chain.

$$C = [CL_1 \quad CL_2 \quad \dots \quad CL_n] \tag{6}$$

The corresponding freedom space, S, is related to the constraint space of the mechanism through the Reciprocal Product as shown in Eq. 7.

$$C\Delta S = 0 \tag{7}$$

The null space of the matrix $C\Delta$ therefore corresponds to the freedom space of the mechanism.

There are a couple of limitations to this type of Constraint-Based Analysis. One inherent assumption is that each joint is composed of ideal DoFs and DoCs that do not change in nature. Compliant joints, for example, do not have ideal constraints and freedoms and can therefore have motions along nominal DoCs or loading along nominal DoFs. In addition, bodies are assumed to be perfectly rigid. In reality, this is often not the case. These assumptions produce limitations that lead to inadequate analyses in certain mechanisms. Examples of this can be found in Sections 2.7 and 2.8. Furthermore, this analysis only describes a mechanism in a single configuration. Many mechanisms have varied mobilities, including loss of DoFs or DoCs and singularities. These can only be accounted for by additional observations or analysis that reach beyond one configuration of the mechanism.

1.2 Loss of DoFs or DoCs

Configurations in which the End Effector loses DoFs or DoCs are significant and should generally be avoided. They can lead to important instantaneous changes in mobility and loss of control of the mechanism if not properly accounted for. A mechanism can lose DoFs for several reasons, including when redundant constraint lines in the mechanism constraint space become non-redundant and when certain non-redundant freedom lines in serial chains become redundant. When this occurs, the mechanism is no longer able to move freely in a certain direction.

Examples of this phenomenon can be found in Sections 2.3, 2.6, and 2.7.

Similarly, a mechanism can lose DoCs (or equivalently, gain DoFs) for several reasons, including when non-redundant constraint lines in the mechanism constraint space become redundant or when certain redundant freedom lines in a serial chain become non-redundant. The appearance of an uncontrolled DoF may cause the End Effector to move in unintended directions. This can occur in the 3-Spherical Kinematic Chain Parallel Mechanism (Section 2.6).

1.3 Singular Configurations

Singular configurations are another important consideration for the mobility of parallel mechanisms. Singularities do not necessarily correspond to a change in the DoFs or DoCs of an End Effector but instead are related to the relationship between mechanism inputs (i.e. actuations) and outputs (i.e. motion of the End Effector). In most configurations, the actuation inputs into a mechanism can be mapped directly to outputs of the End Effector (i.e. forward kinematic problem) or vice versa (i.e. inverse kinematic problem). However, this is not the case in singular configurations. There are three types of singularities that can occur: 1. The inverse kinematic problem fails, 2. The forward kinematic problem fails, or 3. Both problems fail simultaneously [39,40]. Mathematically, the kinematic problem can be defined from the relationships between input and output coordinates shown in Eq. 8, where θ represents the orientations of actuated joints (i.e. inputs) and x represents the End Effector orientation (i.e. outputs). This relation and the results through Eq. 10 are adapted from [39].

$$F(x, \theta) = 0 \tag{8}$$

From this, we can differentiate the kinematic relationships with respect to time to get the relationship shown below:

$$A\dot{x} + B\dot{\theta} = 0 \tag{9}$$

Where

$$A = \frac{\partial F}{\partial x}, \quad B = \frac{\partial F}{\partial \theta} \tag{10}$$

For a mechanism with n degrees of freedom, both A and B are $n \times n$ Jacobian matrices.

The first type of singularity, failure of the inverse kinematic problem, can be expressed using the relationship shown in Eq. 9. We can form the inverse kinematic relationship by inverting the matrix B as in Eq. 11.

$$\dot{\theta} = -B^{-1}A\dot{x} \tag{11}$$

The mechanism will therefore be in a singular configuration of the first type when the matrix B is noninvertible. This is equivalent to saying that the set of actuation inputs needed to achieve the specified End Effector configuration is indeterminate. It can occur if the desired orientation is outside of the mechanism workspace or if the End Effector has reached a special configuration within the workspace [39]. For the latter, intuitively this means that a specified End Effector orientation does not correspond to just one set of inputs. Equivalently, multiple actuation inputs can lead to the same End Effector configuration. One example of this type of singular configuration can be seen when the RRRR 4-bar linkage is in an input toggle configuration, as shown in Fig. 4b. In this configuration, locking the output of the linkage would not prevent the input from moving. The input can therefore be in multiple orientations for the same output configuration. An additional example is shown in the RRRP 4-bar linkage shown in Fig. 4e; this can also occur in the Agile Eye Mechanism (Section 2.3). While the output also loses a DoF in these examples, the mechanism is only singular for the reasons stated above. In general, these two phenomena do not have to occur together. This occurs in the Dual Arch mechanism (Section 2.1), where the mechanism can be singular despite the End Effector not losing any DoFs.

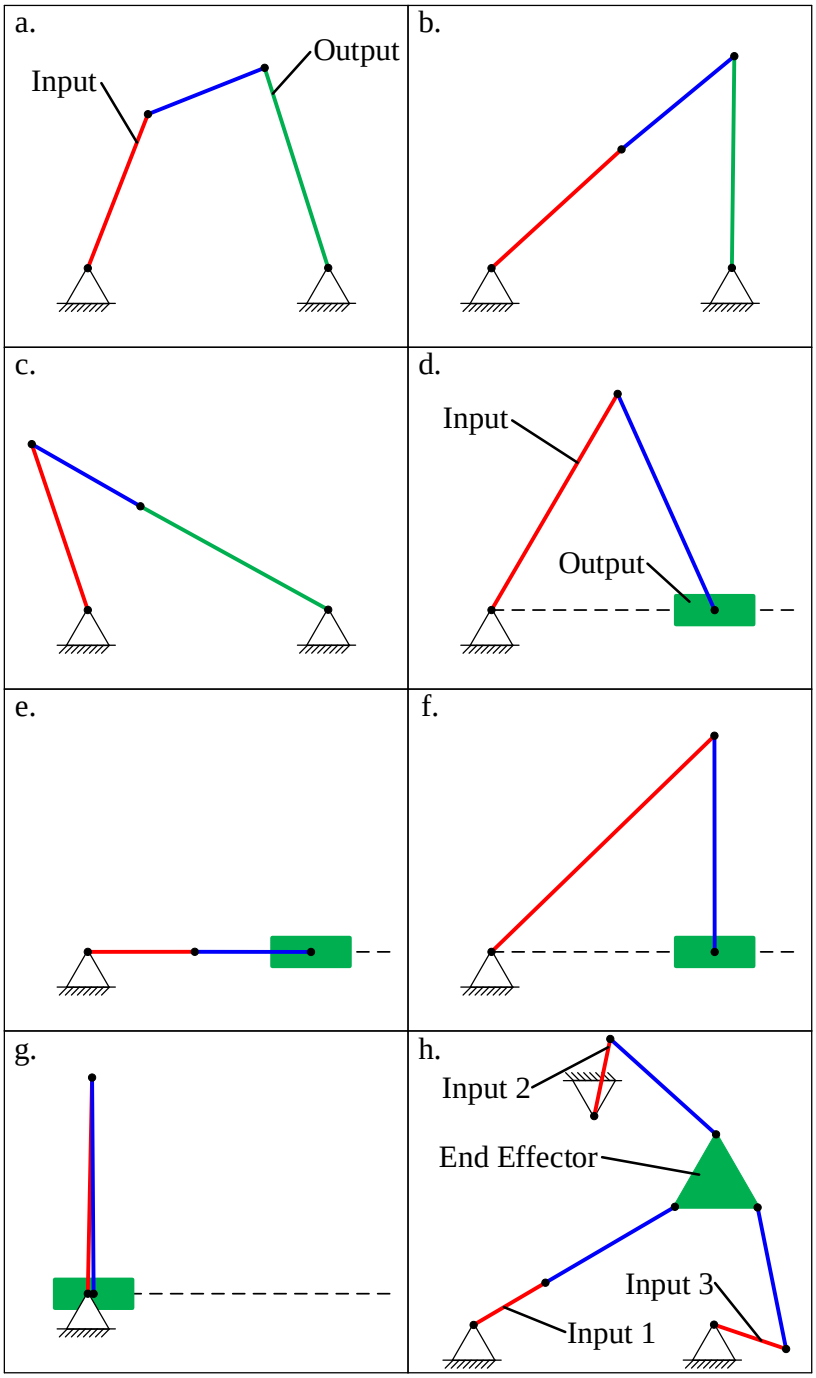

Fig. 4 Examples of Singularities in Mechanisms: a. Example of RRRR 4-bar Linkage, b. First Type of Singularity in RRRR 4-bar Linkage, c. Second Type of Singularity in RRRR 4-bar Linkage, d. Example of RRRP 4-bar Linkage, e. First Type of Singularity in RRRP 4-bar Linkage, f. Second Type of Singularity in RRRP 4-bar Linkage, g. Third Type of Singularity in RRRP 4-bar Linkage, h. Third Type of Singularity in 3RRR Planar Parallel Kinematic Mechanism

The second type of singularity occurs when the forward kinematic problem fails. This problem can be expressed from Eq. 9 by inverting the matrix A to find the equation:

$$\dot{\mathrm{x}} = -A^{-1}\mathrm{B}\dot{\theta} \tag{12}$$

This shows that the mechanism will be in the second type of singular configuration when A is noninvertible. Equivalently, the End Effector orientation obtained by a specified set of actuation inputs is indeterminate. This only occurs within the workspace of the mechanism [39] and when a specified set of actuation outputs does not correspond to just one End Effector orientation. Thus, locking all actuation inputs would not prevent the End Effector from moving. An example of this can be seen in the RRRR 4-bar linkage in Fig. 4c, which is in the output toggle configuration. This type of singularity can also occur in the RRRP 4-bar linkage as shown in Fig. 4f. In both examples, locking the input of the linkage will not prevent the output from being able to move. The output also does not lose a DoC or DoF in both cases. However, displaced configurations in which the End Effector gains DoFs would be examples of this type of singular configuration unless the inverse kinematic problem also fails (third type of singularity). There would now be more DoFs than inputs and locking the set of inputs would not prevent the End Effector from displacing in certain directions. This can occur in the 3-Spherical Kinematic Chain Parallel Mechanism (Section 2.6) when the End Effector gains a DoF.

The third and final type of singularity occurs when both the forward and inverse kinematic problems fail. This is equivalent to matrices A and B being noninvertible simultaneously. As a result, locking all inputs would not prevent the End Effector from displacing and vice versa. An example of this type of singularity can be found in the RRRP 4-bar linkage as shown in Fig. 4g. In this case, the input or output can still move if the other is locked. The third type of singularity also occurs in the 3RRR planar parallel kinematic mechanism

shown in Fig, 4h. In this case, locking the three outputs would not prevent the End Effector from moving; locking the End Effector would also not prevent Input 1 from rotating. This type of singularity is not found in the mechanisms analyzed in this thesis. However, several other examples of each type of singularity can be found in [39,40,43].

CHAPTER 2

Constraint-Based Analysis of Articulated Wrist Mechanisms

The convention of illustrating constraint and freedom lines used throughout this thesis is as follows. Red dashed straight lines are used to indicate rotational DoFs while translational DoFs are shown as red dashed circles that are understood to be of infinite radius. The direction of translation is along the line normal to the plane of this circle. Screw DoFs are shown as solid green lines and constraint lines are shown as solid blue lines. Black center lines are used occasionally to denote axes of interest, but do not indicate any DoFs or DoCs. Letters F and C denote freedom and constraint lines, respectively, and numbers provide further specification. For example, $F1_2$ represents the second freedom offered by the first chain in the parallel kinematic mechanism. Unless otherwise specified, all links and joint are assumed to be ideal – the links are infinitely rigid (or stiff) in all directions, the joints are infinitely stiff in DoC directions, and the joints have zero stiffness and no motion restriction in their DoF directions.

2.1 Dual Arch Mechanism

The dual arch mechanism (Fig. 5a) consists of two identical serial chains. The first chain is made up of a revolute joint R1 that connects the Base to the Arch Link L1; a sliding joint J1 connects Arch Link L1 to the End Effector. The freedom and constraint spaces of this first chain are shown in Fig. 5b. The revolute joint R1 provides the rotational DoF $F1_1$. Sliding joint J1 provides a total of four DoFs. The first is $F1_2$, which lies normal to the plane T1 that runs along

the length of the sliding joint J1. $F1_3$ is a translation along the axis of R1 while $F1_4$ is a translation along the central axis. The final rotation, $F1_5$, is collinear to the central axis. The first chain therefore contributes one constraint, $C1_1$, as dictated by the Rule of Complementary Patterns, to the overall mechanism. This constraint line is parallel to $F1_2$, $F1_3$, and $F1_4$ and passes through the intersection of $F1_1$ and $F1_5$.

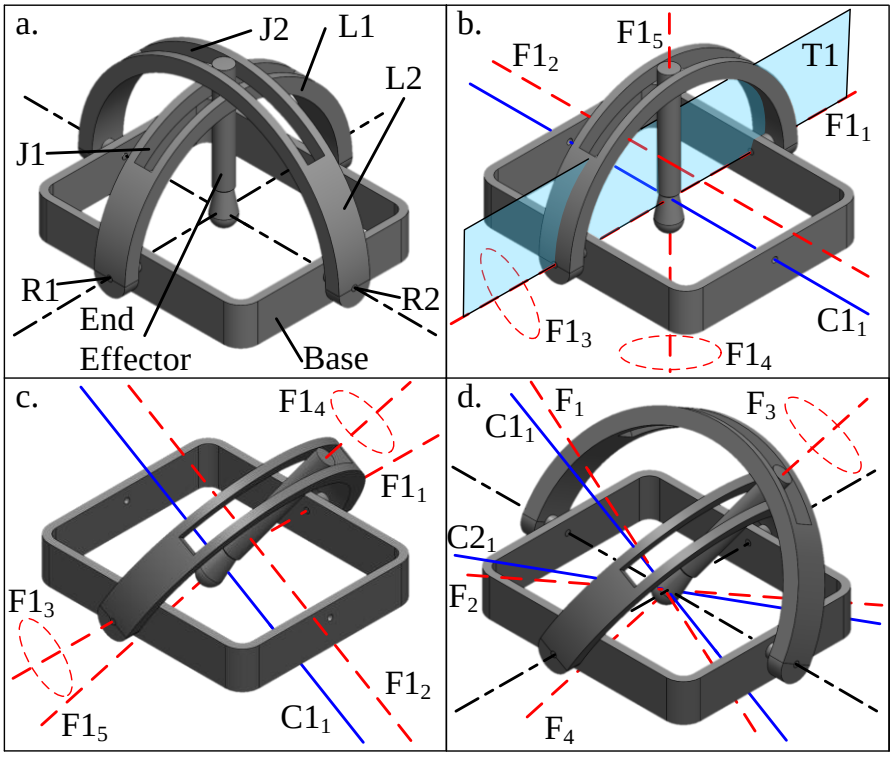

Fig. 5 Dual Arch Mechanism: a. Full mechanism nominal configuration, b. First chain nominal configuration, c. First chain displaced configuration, d. Full mechanism displaced configuration

Fig. 5c illustrates the freedom and constraint spaces of the first chain when the arch has been rotated about the revolute joint R1. While $F1_1$ and $F1_3$ do not move, the freedom lines $F1_2$ and $F1_4$ rotate to maintain their relationships to plane T1 and the End Effector, respectively. $F1_5$ also rotates with the End Effector. The resulting constraint line $C1_1$ in the displaced configuration remains parallel to $F1_2$, $F1_3$, and $F1_4$ and passes through the intersection of $F1_1$ and $F1_5$.

The second chain is orthogonal to the first chain in placement but identical in structure, and therefore has analogous freedom and constraint spaces. With this knowledge, we can construct the mechanism constraint and freedom spaces in a displaced configuration, shown in Fig. 5d. The revolute joint R2 has an axis that passes through the intersection of the R1 axis and the central axis. $C2_1$, contributed by the second chain intersects $C1_1$ at the same point as the intersection point of the R1 and R2 revolute joint axes (illustrated in black). When the End Effector has been rotated in both pitch and yaw, the two constraint lines $C1_1$ and $C2_1$ for the overall mechanism continue to intersect at the intersection point of the R1 and R2 joint axes. As a result, three independent DoFs F_1, F_2, and F_4 for the overall mechanism also pass through this intersection point and form the same freedom space of an ideal spherical joint. Another freedom line, F_3, lies in the plane normal to the central axis. This line can be moved to a point infinitely far away to represent translation of the End Effector along the central axis. Therefore, this mechanism, in the illustrated form, offers 4 DoFs.

F_3 can be removed by constraining the End Effector w.r.t. either or both Arch Links in translation along the central axis while F_4 can be removed by introducing a rotational DoC between the End Effector and only one of the sliding joints. With these additional constraint lines in place, F_1 and F_2, the two remaining DoFs, still lie in the plane normal to the central axis in any displaced configuration. The intersection point of these two freedom lines also does not drift from the intersection point of R1 and R2 axes.

This mechanism has a relatively compact and simple structure, but its range of motion is limited by singular configurations when either of the two Arch Links reaches 90° in any direction. When the mechanism is increasingly articulated in one rotational DoF, the approaching singularity causes a loss in transmission ratio in the other rotational DoF. This means that the

End Effector can no longer be actuated along the second DoF, corresponding to the first type of singularity in Section 1.3. As the transmission ratio drops, the mechanical advantage goes up, which can be beneficial for load transmission. Load bearing capabilities along the DoCs are similarly affected as the mechanism moves from its nominal to a displaced configuration. When the mechanism is articulated in one DoF (e.g. corresponding to R1 joint), the translational DoC along the R1 axis becomes stronger because the End Effector moves closer to the base and therefore the R2 joint axis that supports this DoC. The mechanism's physical limitations (i.e. collisions) and singularities prevent it from tracing out an entire hemisphere but it can trace out a section of this hemisphere around the nominal configuration. Within this continuous but finite range of motion, the load transmission and bearing capabilities are dictated more by the geometry and construction of the various rigid links and joints, which can be designed to suit the application. Furthermore, this mechanism offers a large open space around the intersection of the pitch and yaw axes, making this mechanism suitable not only for pointing and tracking applications, but also applications that require a remote center of rotation located in an open space [6,10–12,20].

2.2 Tip-Tilt Plate Mechanism

The Tip-Tilt Plate mechanism is part of a group of parallel kinematic mechanisms that are similar to the Stewart platform in architecture but offer fewer DoFs. The particular version shown in Fig. 6a, is composed of three outer chains and one central chain and is 3PSS+U. The first outer chain is composed of a prismatic joint $P1_1$ that connects the Base to link $L1_1$. $L1_1$ is connected to $L1_2$ via the spherical joint $S1_1$. $S1_2$ connects $L1_2$ to the End Effector. The central chain is composed of a single universal joint. Revolute joint $R4_1$ connects the Base to the yoke

link $L4_1$, which is connected to the End Effector by $R4_2$.

The freedom space of the first outer serial chain in the nominal configuration is shown in Fig. 6b. $P1_1$ provides the DoF $F1_1$ while $S1_1$ provides $F1_2$, $F1_3$, and $F1_4$. $S1_2$ also provides $F1_4$ as well as $F1_5$ and $F1_6$. The freedom space of this serial chain therefore provides six independent DoFs and has no DoCs.

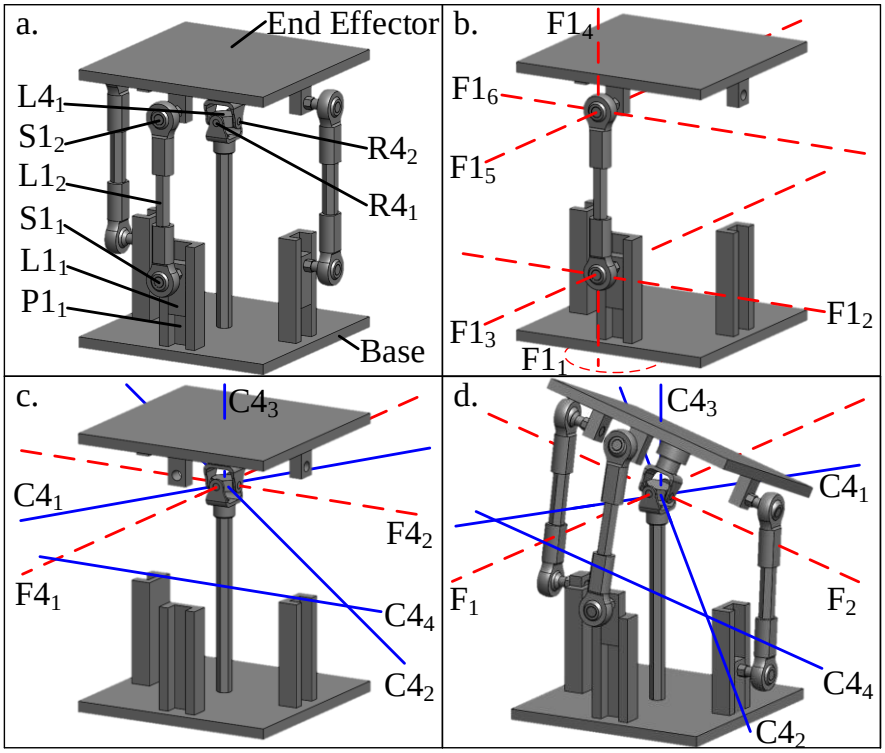

Fig. 6 Tip-Tilt Plate Mechanism: a. Full mechanism nominal configuration, b. First outer chain nominal configuration, c. Central chain nominal configuration, d. Full mechanism displaced configuration

The freedom and constraint spaces of the central chain are shown in Fig. 6c. $R4_1$ and $R4_2$ provide the DoFs $F4_1$ and $F4_2$, respectively. Since these two revolute joints form a universal joint, the freedom lines intersect at a point along the central axis. The corresponding constraint space is therefore composed of four constraint lines. $C4_1$, $C4_2$, and $C4_3$ intersect the same point as the two freedom lines and are not coplanar. $C4_4$ lies in the same plane as the two DoFs but

does not pass through their intersection.

Since the central chain is the only chain with any DoCs, the constraint space of the mechanism is identical to the central chain's in both the nominal and displaced configurations, as shown in Fig. 6d. As a result, this mechanism has two DoFs F_1 and F_2 that are coplanar to $F4_1$ and $F4_2$ and share the same intersection point. While the two freedom lines do not remain in the same plane as the End Effector, their intersection does not drift, and their nature does not change in any displaced configuration. This mechanism can therefore trace out a portion of a hemisphere but is typically limited in range of motion by the joints it is composed of. In cases where joint capabilities do not limit performance, geometric limitations such as link thickness prevent this mechanism from tracing an entire hemisphere.

Load transmission and load bearing capabilities are similarly limited by the capabilities of the joints but can be made very large by increasing their size along with the links. The central chain is especially important to these capabilities since it provides the four DoCs of the mechanism. Although the outer chains do not provide any DoCs, they are important because they provide the opportunity to have independent ground-mounted actuation for each DoF. In this mechanism, this can be done by interfacing the prismatic joints in two orthogonal outer chains with linear actuators (e.g. the first outer chain and one additional chain). The third outer chain as well as any additional outer chains are redundant but could provide the ability to use multiple actuators for a single DoF. Since the central chain defines the DoFs of the mechanism, it is possible to change the DoFs of the mechanism simply by adding or removing joints. For example, introducing a prismatic joint oriented vertically at the base of the central chain would provide a vertical translational DoF to the End Effector [23]. There are several well-known variations of this mechanism, which can have different outer chains (e.g. SPS [23], UPS [5,24],

RSS [21,22], etc.) or central chains (e.g. S [3–5,22], PS [23], etc.). Depending on the variation, rotary actuators may be used (e.g. at the revolute joint of RSS chains) [21,22]. It is also possible to replace the outer chains with cables that can be pulled and released [3,4]. Cables on opposing sides of the central chain can provide the same six DoFs and similar prismatic actuation. These variations can have similar or additional DoFs but may have different tradeoffs including loss of ground-mounted actuation capabilities or higher load transmission and load bearing capabilities. The performance attributes of the 3PSS+U mechanism are attractive for a wide range of applications, including in pointing and tracking applications, rehabilitative robotics, minimally invasive surgery, and additional applications that require large loads. However, the arrangement of its central chain means it does not have an open space around the intersection of its pitch and yaw axes and it therefore cannot be used in applications requiring a remote center of rotation.

2.3 Agile Eye Mechanism

The Agile Eye mechanism is representative of a class of 3RRR spherical parallel kinematic manipulators capable of pitch, yaw, and roll rotations. Numerous other examples of mechanisms with the same kinematic architecture exist within the literature [15,36,44–47]. However, the Agile Eye stands apart because its geometry enables a relatively large workspace that can be arranged to avoid singularities [15,44].

This mechanism is composed of three identical serial chains. The structure of the first serial chain, highlighted in pink, is shown in Fig. 7a. Revolute joint $R1_1$ connects the Base to the first link $L1_1$, which is made up of two circular arc sections that are rigidly connected. $R1_2$ connects $L1_1$ to $L1_2$, which is made up of only one circular arc section. Finally, $R1_3$ connects $L1_2$ to the End Effector.

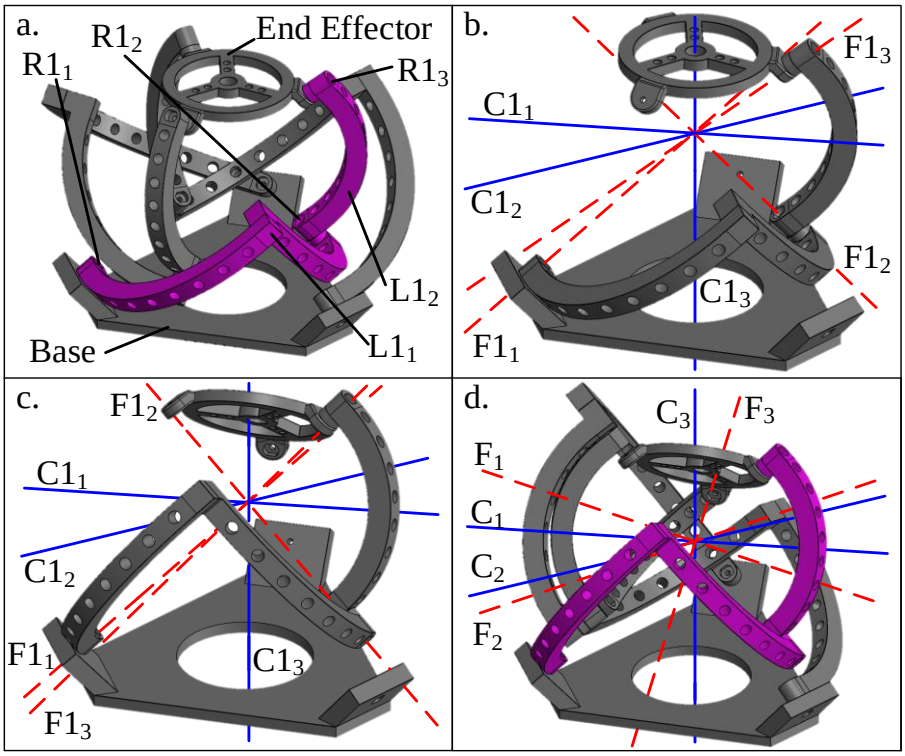

Fig. 7 Agile Eye Mechanism: a. Full mechanism nominal configuration, b. First chain nominal configuration, c. First chain displaced configuration, d. Full mechanism displaced configuration

The constraint and freedom spaces of the first chain in the nominal and displaced configuration are shown in Figs. 7b and 7c, respectively. These illustrate the most important physical detail of this mechanism, which is that the axes of rotation of all nine revolute joints always intersect the same point in space regardless of displacement. They also show the second important physical detail of the Agile Eye: the links are arranged such that F_1 and F_2 are orthogonal and F_2 and F_3 are also orthogonal. In most nominal and displaced configurations, $F1_1$, $F1_2$, and $F1_3$ intersect the same point but are not coplanar. However, the chain loses a DoF and the mechanism becomes singular when $F1_1$ and $F1_3$ are collinear and the three freedom lines are coplanar. These orientations correspond to the first type of singularity as locking the End Effector would not prevent the first link of the chain (e.g. $L1_1$) from rotating [44]. In nonsingular configurations, the DoFs create a corresponding constraint space with three constraint lines $C1_1$,

$C1_2$, and $C1_3$ that also intersect the same point and are not coplanar.

Since the freedom lines of all three chains share the same intersection point, there are six redundant DoCs. The resulting constraint and freedom spaces of the overall mechanism in the displaced configuration are shown in Fig. 7d. Since the mechanism's freedom space comprises three rotational freedom lines that share the same intersection point and are not coplanar, it behaves like an ideal spherical joint. If the mechanism is designed carefully, the freedom space remains unchanged throughout the mechanism's workspace [15]. However, some versions of this mechanism can contain singular configurations within their workspace. These singularities can lead to both the first (see above) and second types of singularity [44].

The strict geometric requirements of joint DoFs intersecting at the same point and complex intertwined architecture that are required place unique practical limitations on the mechanism's performance. Apart from any singularities that can typically be avoided, the reachable workspace in all three DOFs is dictated by collisions between the links and is therefore inversely related to their size (e.g. thickness). Similarly, load transmission and load bearing capabilities are directly related to the size and stiffness of the links. One instance of this mechanism has been shown to achieve a workspace of a 140° cone of constant radius with ±30° in roll [15]. This mechanism does not offer a large open space around the center of rotation (defined by the intersection of the DoFs) over the entire range of motion. This makes this mechanism more suitable for fast pointing and tracking applications than for human interface applications.

2.4 OmniWrist III Mechanism

OmniWrist mechanisms offer singularity-free articulation over large ranges of motion

[13,16,42]. The OmniWrist III is one such example that in its most basic form, consists of three identical chains that are wrapped around the End Effector. However, additional chains can be added while preserving the freedom space and improving the load bearing and transmission capabilities. Accordingly, we present a four-chain version of the OmniWrist III in Fig. 8.

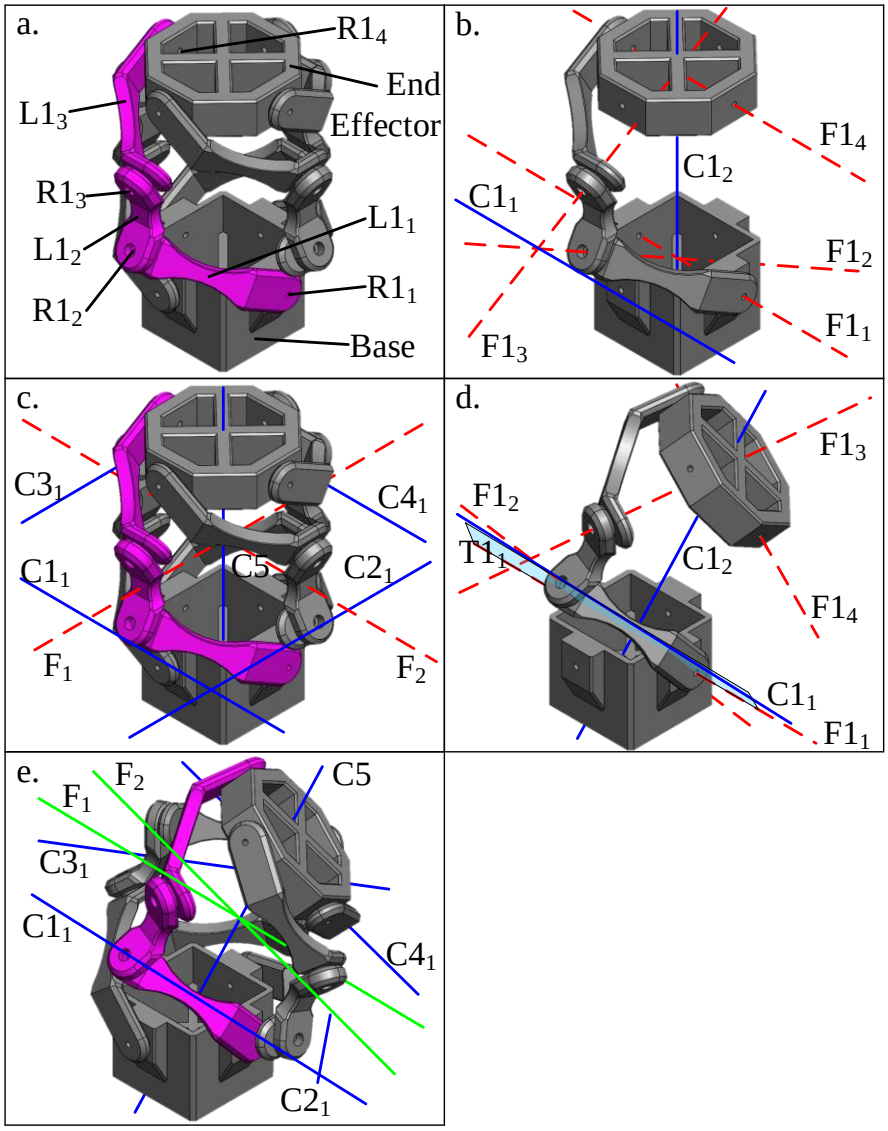

Fig. 8 OmniWrist III Mechanism: a. Full mechanism nominal configuration, b. First chain nominal configuration, c. Full mechanism nominal configuration, d. First chain displaced configuration, e. Full mechanism displaced configuration

Each chain consists of three links connected by four revolute joints. The structure of the first chain, highlighted in pink, is shown in Fig. 8a. Revolute joint $R1_1$ connects the Base to link $L1_1$ and $R1_2$ connects this link to $L1_2$. $R1_3$ connects $L1_2$ to $L1_3$ which is connected to the End Effector via $R1_4$.

The freedom and constraint spaces of the first chain in the nominal configuration are shown in Fig. 8b. Each revolute joint in the chain provides the freedom line with identical numbering. The most important feature of this mechanism is that $F1_1$ and $F1_2$ intersect at a point at the center of the base and $F1_3$ and $F1_4$ intersect at the center of the End Effector. This is possible because of the special construction of links $L1_1$ and $L1_3$, which are identical; these two freedom line intersections remain in the same location of the Base and End Effector regardless of mechanism orientation. The constraint line $C1_2$ is therefore the line that connects these two intersections. $F1_2$ and $F1_3$ also intersect at a point outside of the mechanism because of the special construction of $L1_2$. Constraint line $C1_1$ is the line that passes through this freedom line intersection and is also parallel to $F1_1$ and $F1_4$.

The constraint and freedom spaces of the overall mechanism in the nominal configuration are shown in Fig. 8c. C_5 is collectively composed of $C1_2$, $C2_2$, $C3_2$, and $C4_2$, which are redundant. If the special link relations created by the geometry of the first and third links (e.g. $L1_1$ and $L1_3$) did not hold for all four chains, the four constraints would not be redundant and this mechanism may not be able to pitch or yaw. Since $C1_1$, $C2_1$, $C3_1$, and $C4_1$ are coplanar, one of the constraints is redundant. The mechanism therefore has four independent constraints and produces a freedom space of F_1 and F_2 that are coplanar to $C1_1$, $C2_1$, $C3_1$, and $C4_1$ and intersect C_5. These freedom lines do not have to be orthogonal and are only illustrated in this way for convenience. This freedom space represents the pitch and yaw rotations of an articulated wrist

mechanism. However, it does not maintain this freedom space in displaced configurations.

Fig. 8d shows the freedom and constraint spaces of the first chain in a displaced configuration. $F1_1$, $F1_2$, and $F1_3$ maintain similar relationships to each other while $F1_4$ rotates along with the End Effector. As a result, $F1_4$ is no longer parallel to $F1_1$, which had made it straightforward to identify $C1_1$. In order to find $C1_1$, it is useful to first construct the plane $T1_1$. This plane contains $F1_1$ and the point of intersection between $F1_2$ and $F1_3$. $C1_1$ is the line lying in $T1_1$ that passes through the intersection point between $F1_2$ and $F1_3$ and the intersection point between $F1_4$ and $T1_1$. This constraint line will also naturally intersect $F1_1$ because it lies in $T1_1$ and therefore intersects every freedom line. While the orientation of $F1_4$ changes relative to $F1_1$, the intersection points of $F1_1$ and $F1_2$, $F1_2$ and $F1_3$, and $F1_3$ and $F1_4$ are preserved as expected. Thus, $C1_2$ still passes through the same points on the Base and End Effector.

Since $C1_1$, $C2_1$, $C3_1$, and $C4_1$ are no longer coplanar and have more complicated relationships, it is difficult to draw the corresponding freedom space. It is therefore simpler to use screw theory directly to conduct the constraint analysis. The constraint and freedom spaces in the displaced configuration are shown in Fig. 8e. C_5 still collectively represents the redundant constraint lines $C1_2$, $C2_2$, $C3_2$, and $C4_2$. The mechanism's freedom space is composed of two screws that appear to intersect each other and remain perpendicular to C_5. The intersection point also remains a constant distance from the End Effector, meaning that while the nature of the DoFs changes, their location does not drift. However, given the numerical approach used to determine the freedom space, these attributes could not be confirmed geometrically. The FACT catalog helps to identify the constraint space as nested circular hyperboloids [33]. This occurs because of the symmetry of the mechanism, which enables the DoCs of one serial chain to be redundant in all displaced configurations. It is therefore feasible to use three serial chains instead

or introduce additional serial chains as long as the symmetries needed to produce this freedom space are maintained.

Because its freedom space comprises two intersecting screws in displaced configurations, the OmniWrist III is unable to trace out a perfect hemisphere. However, it can trace out an oblong hemisphere (full 180º) while remaining free of singularity. Compared to many of the other articulated wrist mechanism options discussed in this thesis, the OmniWrist III has a unique aspect ratio – greater height and narrow width, which might be advantageous in certain tight-space applications. Actuation of this mechanism is typically done via rotation of the first links of two chains (e.g. $L1_1$ about the joint $R1_1$). The mechanism can be actuated through its full 180° hemispherical range of motion with smaller rotations of the first links, which allows for the use of limited stroke rotary or linear actuators.

The mechanism's range of motion is determined by collision between links from different chains. This results in a tradeoff between link dimensions (e.g. thickness) and the range of motion. To maximize range of motion, the links must be compact; this can also result in finite stiffness of the supposedly rigid links. This adversely impacts load bearing and transmission capabilities. In particular, the load bearing capability along constraint line C_5 is sensitive since it depends on the bending stiffness of the serially connected links (e.g. $L1_1$-$L1_2$-$L1_3$). These features and tradeoffs make this mechanism a promising candidate in applications including pointing, tracking, and manufacturing. In the latter application, a robotic arm that supports the mechanism can make up for the small translations caused by the screw DoFs. It is also possible to arrange the serial chains to create an open space around the intersection of the two DoFs. This mechanism can therefore also be used in applications that require a human interface.

2.5 OmniWrist V Mechanism

While the OmniWrist V and VI may appear architecturally different from the OmniWrist III, a constraint-based analysis reveals the similarities between these two mechanisms. The former is shown in Fig. 9a and consists of two different types of chains. The first chain is an example of the outer chain. A revolute joint $R1_1$ connects the Base to link $L1_1$. A spherical joint $S1_1$ connects link $L1_1$ to link $L1_2$ which is connected to the End Effector via revolute joint $R1_2$. The fourth chain in the mechanism is the central chain. It consists of a spherical joint $S4_1$ that connects the Base to link $L4_1$ which is connected to the End Effector via spherical joint $S4_2$.

The freedom and constraint spaces of the first outer chain in the nominal configuration are shown in Fig. 9b. $R1_1$ provides the freedom line $F1_1$, spherical joint $S1_1$ provides $F1_2$, $F1_3$, and $F1_4$, and $R1_2$ provides $F1_5$; this adds to a total of five DoFs. The corresponding constraint line $C1_1$ must pass through the center of $S1_1$ in order to intersect $F1_2$, $F1_3$, and $F1_4$. It also must run parallel to $F1_1$ and $F1_5$.

The freedom and constraint spaces of the central chain in the nominal configuration are shown in Fig. 9c. Both $S4_1$ and $S4_2$ provide three DoFs. However, one of the DoFs is redundant and is represented by the shared freedom line $F4_3$. The resulting single constraint line $C4_1$ is the line drawn between the centers of the two joints. This relation holds throughout the mechanism's workspace.

With an understanding of the constraint lines provided by each chain in the nominal configuration, the nominal mechanism constraint space can be drawn as shown in Fig. 9d. This reveals that the constraint lines formerly provided by a single serial chain in the OmniWrist III are decoupled into two separate chains in this mechanism. The outer serial chains provide constraint lines similar to $C1_1$ in the OmniWrist III while C_5 is now provided by a single central

chain. $C1_1$, $C2_1$, and $C3_1$ are coplanar in the nominal configuration and therefore any two freedom lines lying within the same plane and also intersecting $C4_1$ can be chosen. Thus, this mechanism also provides pure pitch and yaw rotational DoFs in the nominal configuration but does not maintain this freedom space in displaced configurations.

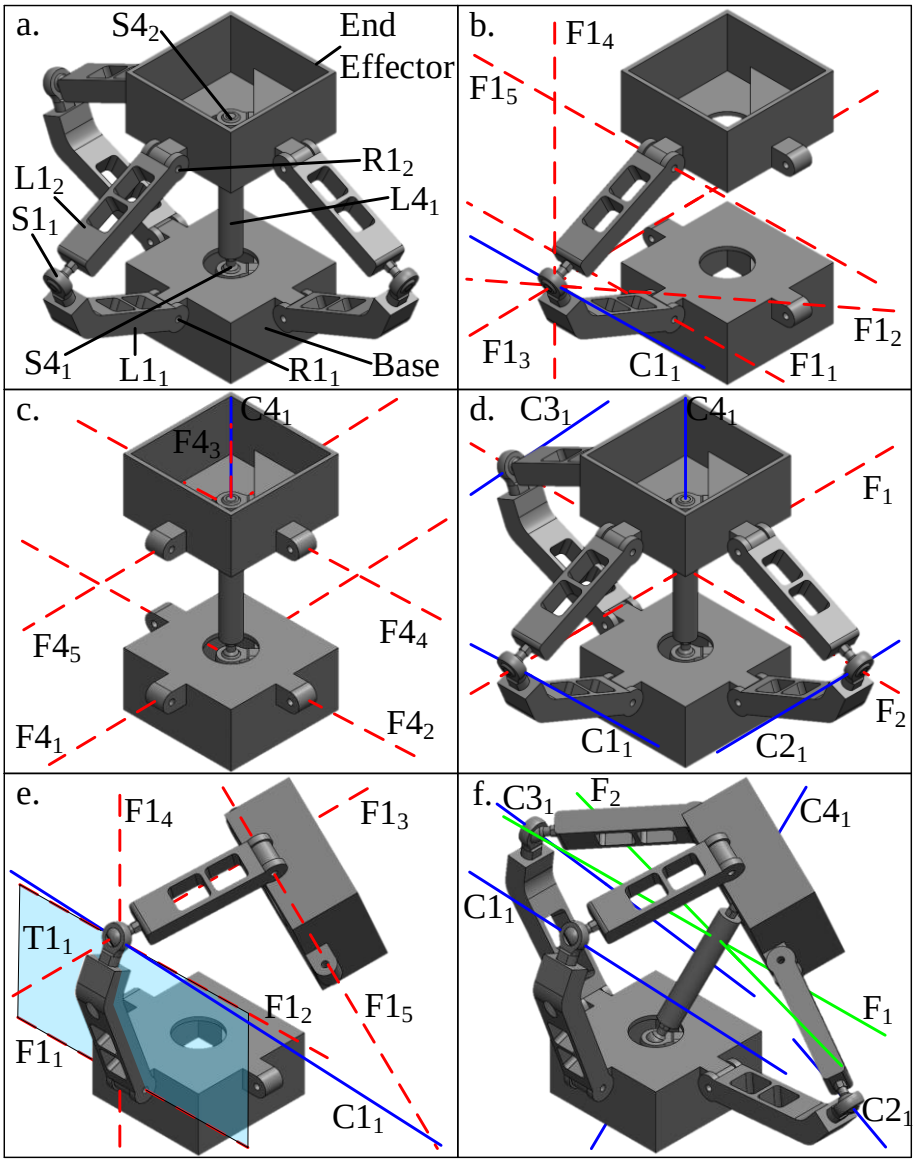

Fig. 9 OmniWrist V Mechanism: a. Full mechanism nominal configuration, b. First outer chain nominal configuration, c. Central chain nominal configuration, d. Full mechanism nominal configuration, e. First chain displaced configuration, f. Full mechanism displaced configuration

The freedom and constraint spaces for the first outer chain in the displaced configuration are shown in Fig. 9e. While links $L1_1$ and $L1_2$ become displaced, the relative orientations of freedom lines $F1_1$, $F1_2$, $F1_3$, and $F1_4$ all similar relationships to each other. However, the orientation of $F1_5$ rotates to maintain its relation to the displaced End Effector. As a result, it is useful to apply an analogous approach to that used for the OmniWrist III to identify the constraint line $C1_1$. First the plane $T1_1$ containing $F1_1$ and the center of $S1_1$ is constructed. $C1_1$ is the line lying in this plane that passes through the center of $S1_1$ and the intersection of $T1_1$ with $F1_5$.

As with the OmniWrist III, the changes to the orientations of $C1_1$, $C2_1$, and $C3_1$ mean they are no longer coplanar. A numerical analysis reveals that the corresponding freedom space now consists of two screw lines that appear to intersect each other and $C4_1$ as shown in Fig. 9f. In addition, the plane comprising these two screw lines appears normal to $C4_1$ and does not drift in any displaced configurations. As is the case with the OmniWrist III mechanism, these attributes of the freedom space were observed via a numerical analysis and were not confirmed geometrically. The FACT catalog helps identify the constraint space as nested circular hyperboloids, as with the OmniWrist III [33].

The appearance of screw lines means that this mechanism is also unable to trace out a perfect hemisphere. The central chain plays a critical role in the range of motion of this mechanism, which can be dictated by the spherical joints $S4_1$ and $S4_2$. For the End Effector to span its full hemispherical range, these spherical joints must together provide 90^o of rotation from their nominal configuration. Unlike with the OmniWrist III, in general, high load bearing along DoCs can be achieved via adequately stiff links and joints in the mechanism because of few geometric limitations; links can be made thicker for little cost beyond additional mass. In

addition, the decoupling of DoCs into two different types of chains means that the central chain can provide significant load bearing capability along constraint line $C4_1$ because $L4_1$ is either in tension or compression instead of in bending. This mechanism is therefore better suited for applications requiring high load bearing and transmission stiffness than the OmniWrist III. This makes the mechanism a great candidate for pointing or tracking applications as well as for manufacturing applications such as welding and spray painting. However, the central chain envelops the intersection of the freedom lines and it therefore cannot be used for applications requiring a remote center of rotation located in an open space.

As with the OmniWrist III, the mechanism can be actuated through a full 180° by a limited stroke rotary or linear actuators. In addition, the outer chains in this mechanism can also be spaced 120° apart instead of 90°. Furthermore, as with the OmniWrist III, this architecture allows for the inclusion of additional outer chains, which would be redundant and would not alter the freedom space of the mechanism in any configuration. For example, the OmniWrist VI has a very similar structure compared to OmniWrist V but includes four outer chains instead of three. Thus, while the OmniWrist VI requires tighter manufacturing and assembly tolerances to manage the overconstraint, it will have improved load bearing capabilities due to the additional stiffness of a fourth chain.

2.6 3-Spherical Kinematic Chain Parallel Mechanism

This mechanism bears similarities to both OmniWrist mechanisms, but especially the OmniWrist V because of a similar chain and similar mechanism freedom space. It is composed of at least three identical serial-parallel hybrid chains instead of purely serial chains and is presented with three chains in Fig. 10.

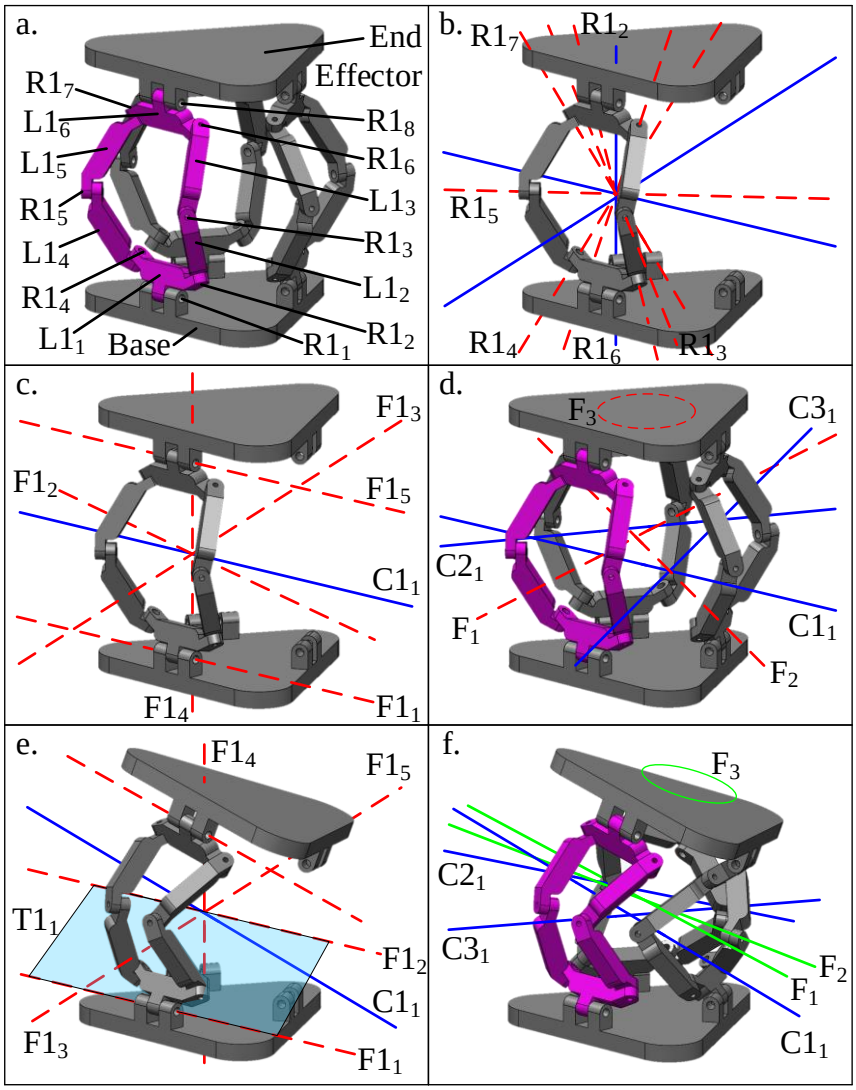

Fig. 10 3-Spherical Kinematic Chain Parallel Mechanism: a. Full mechanism nominal configuration, b. First chain's spherical parallel sub-chain nominal configuration, c. First chain nominal configuration, d. Full mechanism nominal configuration, e. First chain displaced configuration, f. Full mechanism displaced configuration

The structure of the first chain, highlighted in pink, is shown in Fig. 10a and below:

$$\text{B-R1}_1\text{-L1}_1\begin{matrix}\nearrow \text{R1}_2\text{-L1}_2\text{-R1}_3\text{-L1}_3\text{-R1}_6 \searrow \\ \searrow \text{R1}_4\text{-L1}_4\text{-R1}_5\text{-L1}_5\text{-R1}_7 \nearrow\end{matrix}\text{L1}_6\text{-R1}_8\text{-EE}$$

Revolute joint $R1_1$ connects the base to link $L1_1$. This link is connected to two separate serial sub-chains that are arranged in parallel, collectively called the spherical parallel sub-chain. Each

serial sub-chain of the spherical parallel sub-chain consists of three revolute joints connecting two links to $L1_1$ (e.g. $L1_1$ to $R1_2$ to $L1_2$ to $R1_3$ to $L1_3$ to $R1_6$). These two serial sub-chains both connect to $L1_6$ via the final revolute joints in the sub-chains (e.g. $R1_6$). Finally, $R1_8$ connects $L1_6$ to the End Effector.

The constraint and freedom spaces of the first chain's spherical parallel sub-chain are shown in Fig. 10b. An important attribute of each revolute joint is that the DoF it provides passes through the same intersection point. Since the three freedom lines of each serial sub-chain are not coplanar, the serial sub-chain is kinematically equivalent to a spherical joint centered at the intersection point. If the freedom lines are not coplanar, the entire spherical parallel sub-chain and thus the overall first chain will lose a DoF. Assuming these configurations are avoided, one of the two serial sub-chains is redundant.

The constraint and freedom spaces of the first serial chain of the mechanism in the nominal configuration are shown in Fig. 10c. This freedom space is arranged similarly to that of the outer serial chain of the OmniWrist V. $R1_1$ and $R1_8$ provide DoFs $F1_1$ and $F1_5$, similar to the OmniWrist V. However, in this case, freedom lines $F1_2$, $F1_3$, and $F1_4$, provided by a spherical joint in the OmniWrist V, are provided by the spherical parallel sub-chain. The corresponding constraint space consists of a single constraint line passing through the intersection point of the spherical parallel sub-chain and is parallel to $F1_1$ and $F1_8$.

Fig. 10d shows the constraint and freedom spaces of the overall mechanism. Each serial chain provides a single constraint line; the three constraint lines are coplanar but do not share a single intersection point. Therefore, none are redundant, and the mechanism has three corresponding DoFs. If a constraint line does become redundant, the mechanism would gain an additional DoF and would therefore be in the second type of singular configuration. This is

possible upon displacement if the spherical centers of the three sub-chains become coincident. When the mechanism is nonsingular, the three freedom lines lie in the same plane as the constraint lines and do not share the same intersection point. F_1, F_2, and F_3 can therefore represent pitch, yaw, and vertical translational DoFs respectively, as shown in the figure. This freedom space is like the OmniWrist mechanisms' but includes an additional translational DoF. This is because none of the three chains provide a DoC analogous to the one provided by the central chain of the OmniWrist V.

As with the OmniWrist mechanisms, the freedom space of the mechanism changes significantly in displaced configurations. The freedom and constraint spaces of the first serial chain after it has displaced from the nominal configuration in pitch and yaw but not translation are shown in Fig. 10e. Assuming the spherical parallel sub-chain has not lost a DoF, the serial chain still provides 5 independent DoFs. As with the OmniWrist V, it is helpful to construct plane $T1_1$ to identify the constraint line. $T1_1$ passes through the intersection point of the spherical parallel sub-chain and also contains $F1_1$. $C1_1$ lies in $T1_1$ and passes through both the intersection point of the spherical parallel sub-chain and the intersection point of $F1_5$ with $T1_1$.

The constraint lines of the three chains are no longer coplanar when the mechanism is displaced in pitch and yaw without translation. As with the OmniWrist mechanisms, it is convenient to use screw theory to numerically find the corresponding freedom space, shown in Fig. 10f. This analysis shows that the freedom space is composed of three screw lines, of which two screw lines F_1 and F_2 appear to intersect. In addition, the plane they lie in does not drift in any displaced configurations. These screw lines are analogous to the pitch and yaw DoFs from the nominal configuration. The appearance of these screw lines in displaced configurations means that the mechanism is unable to trace a perfect hemisphere. The third screw line, F_3, is

analogous to the translational DoF and it has a very high pitch, unlike the other two screw DoFs. From this pure pitch and yaw displaced configuration, if the mechanism is now displaced in translation, the above described freedom and constraint spaces will no longer apply. This is because the End Effector will also twist about F_3 while translating.

The FACT catalog reveals that this arrangement of three screw DoFs corresponds to a constraint space that takes the shape of a single circular hyperboloid [33]. This only differs from the OmniWrist mechanisms because of the absence of an additional constraint line belonging to a nested circular hyperboloid. This was provided by the central chain in the OmniWrist V and its analog in the OmniWrist III. However, F_3 could be removed with the addition of a chain like the OmniWrist V's central chain or by removing symmetry when a fourth chain is added. The catalog also reveals that an identical fourth chain arranged correctly would be redundant since the constraint line it provides would also be a part of the same circular hyperboloid.

Replacing the OmniWrist V outer serial chain's spherical joint with the spherical parallel sub-chain has several consequences that lead to clear differences between the two mechanisms. The sub-chains can have improved stiffness because of their revolute joints and parallel architecture. In addition, they do not change the overall kinematic behavior of the mechanism in most displaced configurations. However, the mechanism's range of motion is limited by several factors related to the sub-chain including locations leading to loss of DoFs, singularities, or link collisions. There is therefore a tradeoff between range of motion and load bearing and transmission capabilities as these depend on the stiffness and therefore size of the links and joints. Thus, its set of performance tradeoffs is more like that of the OmniWrist III than the OmniWrist V despite its kinematic structure.

This mechanism is well-suited for applications that require a remote center of rotation

located in an open space. It is also suitable for pointing and tracking applications as well as others that do not require high load bearing and transmission capabilities; one instance of this mechanism demonstrated a range of motion of 15°-27° in pitch and yaw in similar applications [1].

2.7 FlexDex® Mechanism

The FlexDex mechanism offers constraint and freedom spaces that are similar to the Dual Arch mechanism but highlights many advantages of compliant elements. The mechanism is composed of two identical chains; the structure of the first chain is shown in Fig. 11a. Revolute joint $R1_1$ connects the Base to link $L1_1$ and revolute joint $R1_2$ connects $L1_1$ to $L1_2$. $L1_2$ is a compliant strip composed of alternating "rigid" sections and compliant hinges. These compliant hinges are initially modeled as ideal revolute joints; the first two of these joints, $H1_1$ and $H1_2$ are labeled in the figure. While an ideal revolute joint has zero motion and infinite stiffness along its DoCs, in practice, a compliant hinge will have finite compliance along its DoF and finite stiffness and parasitic error motion along its DoCs. Similarly, the rigid sections are modeled initially as being ideal (i.e. infinitely stiff) but can have finite stiffness in practice. A revolute joint $R1_3$ connects $L1_2$ to the End Effector.

The freedom and constraint spaces of the first chain in the nominal configuration are shown in Fig. 11b. Each revolute joint and compliant hinge provides a single DoF as expected. An important feature of link $L1_2$ is that the nominal axis of rotation of each compliant hinge is parallel to those of $R1_2$ and $R1_3$. The compliant hinges therefore provide DoFs that are parallel to $F1_2$ and $F1_4$. However, only a maximum of three of these parallel freedom lines are independent and multiple DoFs provided by compliant hinges have been omitted in the figure for simplicity

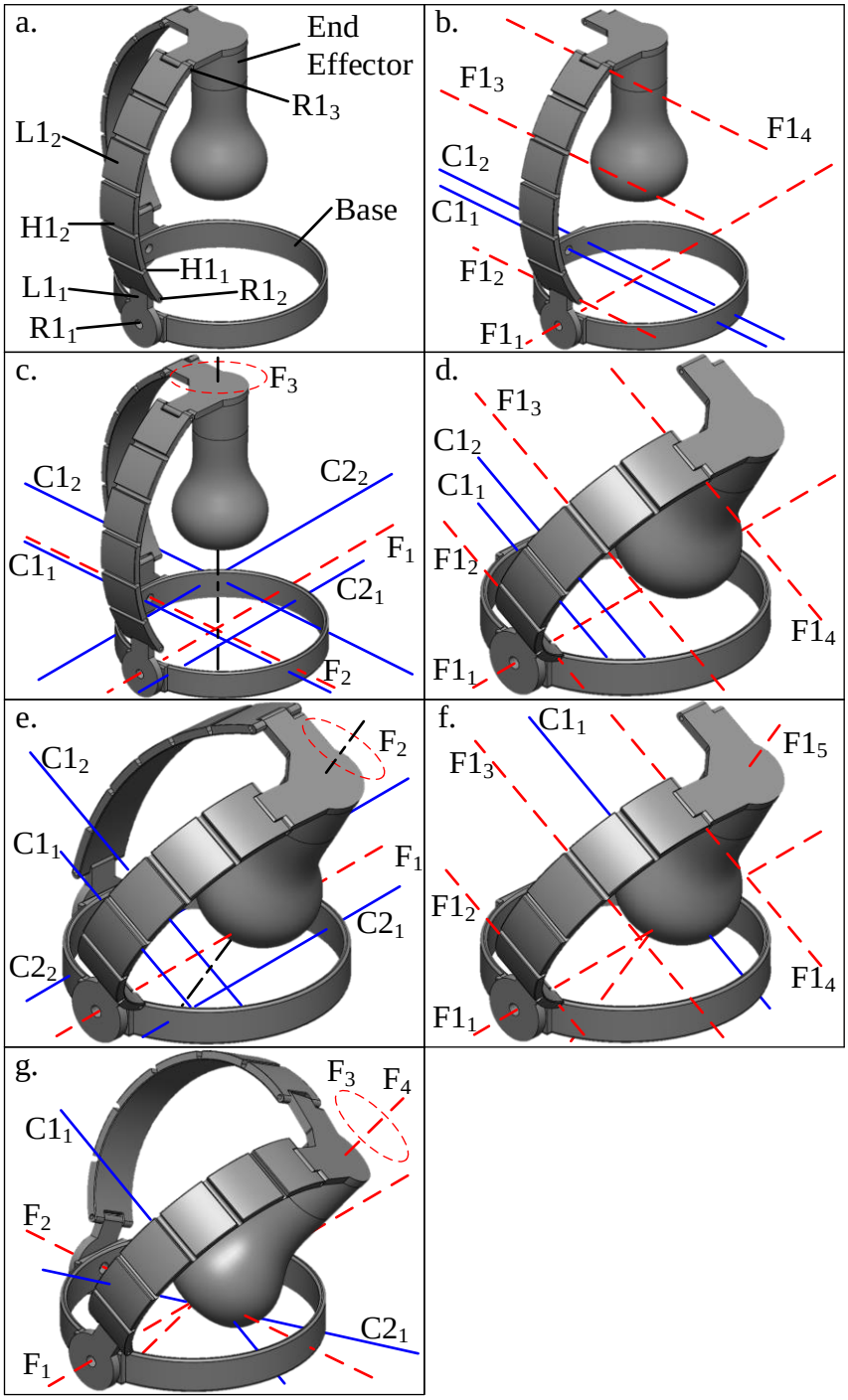

Fig. 11 FlexDex Mechanism: a. Full mechanism nominal configuration, b. First chain nominal configuration, c. Full mechanism nominal configuration, d. First chain after single rotation, e. Full mechanism after single rotation, f. Modified freedom space for first chain after single rotation, g. Full mechanism after both rotations

of illustration. This relationship only holds when the compliant strip is not held flat. In this orientation, $F1_2$, $F1_3$, $F1_4$, and all other DoFs provided by the compliant strip are parallel and coplanar. Only two of these freedom lines would be independent and the End Effector would lose a DoF in this orientation. This issue is inherently avoided by the length and orientation of the two compliant strips in the FlexDex mechanism. Assuming the strip is curved, the first chain provides four independent freedom lines: $F1_1$, $F1_2$, $F1_3$, and $F1_4$. The corresponding constraint space is two lines $C1_1$ and $C1_2$ that are parallel to $F1_2$, $F1_3$, and $F1_4$ and intersect $F1_1$. While these two constraint lines must be coplanar with $F1_1$, the absence of a fifth DoF $F1_5$ in the first chain (which was present in the case of the Dual Arch Gimbal) removes the strict positional requirement for the constraint lines; they can lie anywhere in the plane they share with $F1_1$.

The constraint and freedom spaces of the overall mechanism in the nominal configuration are shown in Fig. 11c. Since the four constraint lines are coplanar, only three are independent. This produces the corresponding freedom space with the three independent freedom lines F_1, F_2, and F_3 that lie in the same plane and do not share the same intersection point. These can be arranged such that F_1 and F_2 correspond to pitch and yaw motions and F_3 corresponds to a vertical translation. This is the expected freedom space of an articulated wrist mechanism with an additional translational DoF. However, the freedom and constraint spaces deviate from this ideal arrangement in displaced configurations of the mechanism.

The freedom and constraint spaces of the first chain after the chain has rotated about $F1_1$ are shown in Fig. 11d. $F1_2$, $F1_3$, and $F1_4$ rotate with their respective revolute joints and compliant hinges. $C1_1$ and $C1_2$ still intersect $F1_1$ but also rotate in order to remain parallel to $F1_2$, $F1_3$, and $F1_4$. The constraint and freedom spaces of the overall mechanism after the first chain has rotated about $F1_1$ are shown in Fig. 11e. The mechanism constraint space now contains four constraint

lines that do not lie in a single plane and are therefore no longer redundant. As a result, the mechanism's freedom space devolves into a 2 DoF space where the freedom lines are parallel to $C2_1$ and $C2_2$ and intersect both $C1_1$ and $C1_2$. These two freedom lines can be arranged so that F_1 corresponds to continued rotation about the same axis (i.e. $F1_1$) and F_2 corresponds to a translation along the central axis. The loss of DoF is critical in this case because the mechanism is no longer an articulated wrist mechanism. However, note that this analysis, and therefore the resulting outcome, is based on an ideal constraint assumption for the compliant hinges, revolute joints, ideal rigid sections, and links.

In practice, the compliant strip is not ideal and compliance is advantageously employed to introduce intentional deviation from ideal behavior. In particular, its "rigid" sections and compliant hinges have finite compliance in torsion (as opposed to zero compliance or infinite stiffness in the ideal scenarios). This compliance plays an important role in providing the desired articulation functionality in this mechanism, as demonstrated in practical use [9,10].

With this knowledge and some modified assumptions, we can analyze the freedom and constraint spaces again. Most importantly, even though torsion is not truly a DoF for the compliant strip, we introduce the freedom line $F1_5$ to recognize the small but finite compliance in this direction. It is logical to place this additional freedom line collinear to the central axis because of the symmetry of the mechanism, although it can be located elsewhere depending on the geometric details of the compliant strip. With this assumption, the resulting freedom and constraint spaces of the first chain after it has rotated about the freedom $F1_1$ are shown in Fig. 11f. This freedom space is identical to the freedom space of the first chain in the Dual Arch in a displaced configuration. The addition of $F1_5$ removes one of the two constraint lines that are present in Fig. 11d. $C1_1$ must now pass through the intersection of $F1_1$ and $F1_5$.

Making a similar non-ideal assumption for the second compliant strip, the constraint and freedom spaces of the overall mechanism after both chains have rotated about $F1_1$ and $F2_1$ respectively are shown in Fig. 11g. The mechanism freedom space now resembles that of an articulated wrist mechanism as F_1 and F_2 correspond to pitch and yaw DoFs. In addition, these two freedom lines do not drift because $C1_1$ and $C2_1$ cannot drift. F_3 represents translation of the End Effector about its central axis as it did when the mechanism was in the nominal configuration. F_4 represents rotation of the End Effector about its central axis, resulting from the small but finite torsional compliance assumption for the compliant strips. However, the stiffness of this DoF will remain higher than in the directions of the other DoFs. Overall, intentional use of compliance in mechanism design highlights the limits of constraint analysis that assumes ideal links and joints.

While intentional compliance provides desired functionality and expands the mechanism design space, it also leads to an inherent set of tradeoffs. Increasing the above torsional compliance of the compliant strips increases the range of articulation but reduces the load bearing and transmission capabilities of the mechanism. Transmission of an actuation load from the first revolute joints (e.g. $R1_1$) to the End Effector will cause the compliant strip to twist, thereby limiting its torque transmission capability. Also, such twisting means that the freedom lines provided by the compliant hinges of $L1_2$ will no longer be parallel and redundant, which impacts the freedom space of the overall mechanism. Similar issues will impact load bearing capabilities along the DoCs of the mechanism. Loading may also cause the torsional freedom line (e.g. $F1_5$) to drift, which in turn would cause F_1 and F_2 to drift. Furthermore, this mechanism stores energy because of its compliance thereby impacting transmission efficiency. However, with suitable optimization of compliance and link and joint dimensions, it is possible for this

mechanism to achieve close to a full hemispherical range of motion.

The mechanism offers a large open space around the center of rotation (i.e. intersection of F_1 and F_2), making it well suited for applications that require a human interface [9,10]. In these types of applications, F_3 enables natural adjustability to ensure the user's wrist is centered at the mechanism's center of rotation regardless of hand size.

2.8 BYU Space Pointing Mechanism

The BYU Space Pointing Mechanism is a novel compliant parallel kinematic architecture [17], shown in Fig. 12a in its nominal configuration. It contains two chains shown in pink and blue that are not identical. A rotary actuator is meant to be connected to each chain via the hexagonal protrusions labeled $M1_1$ and $M2_1$. The first chain, shown in pink, contains four cross-axis flexural pivots, which are meant to approximate revolute joints. $M1_1$ is connected to the first two pivots $H1_1$ and $H1_2$ via rigid link $L1_1$. $H1_1$ and $H1_2$ have collinear axes of rotation. These two flexural pivots are directly connected to the Base, shown in gray. Link $L1_1$ connects $M1_1$, $H1_1$, and $H1_2$ to the other two flexural pivots $H1_3$ and $H1_4$. $H1_3$ and $H1_4$ also have collinear axes of rotation. These two pivots are directly connected to the End Effector, shown in orange. The second chain, shown in blue, consists of two cross-axis flexural pivots $H2_1$ and $H2_2$ as well as one split-tube flexure $H2_3$, which also approximates a revolute joint. The Base is directly connected to $H2_1$, which is connected to M_2 via rigid link $L2_1$. $L2_1$ is also connected to $H2_2$. $H2_3$ is directly connected to both $H2_2$ and the End Effector.

The freedom and constraint spaces of the first chain in the nominal configuration are shown in Fig. 12b. $F1_1$ is provided by both $H1_1$ and $H1_2$ while $F1_2$ is provided by both $H1_3$ and $H1_4$. These two freedom lines are orthogonal and intersect. The corresponding constraint space

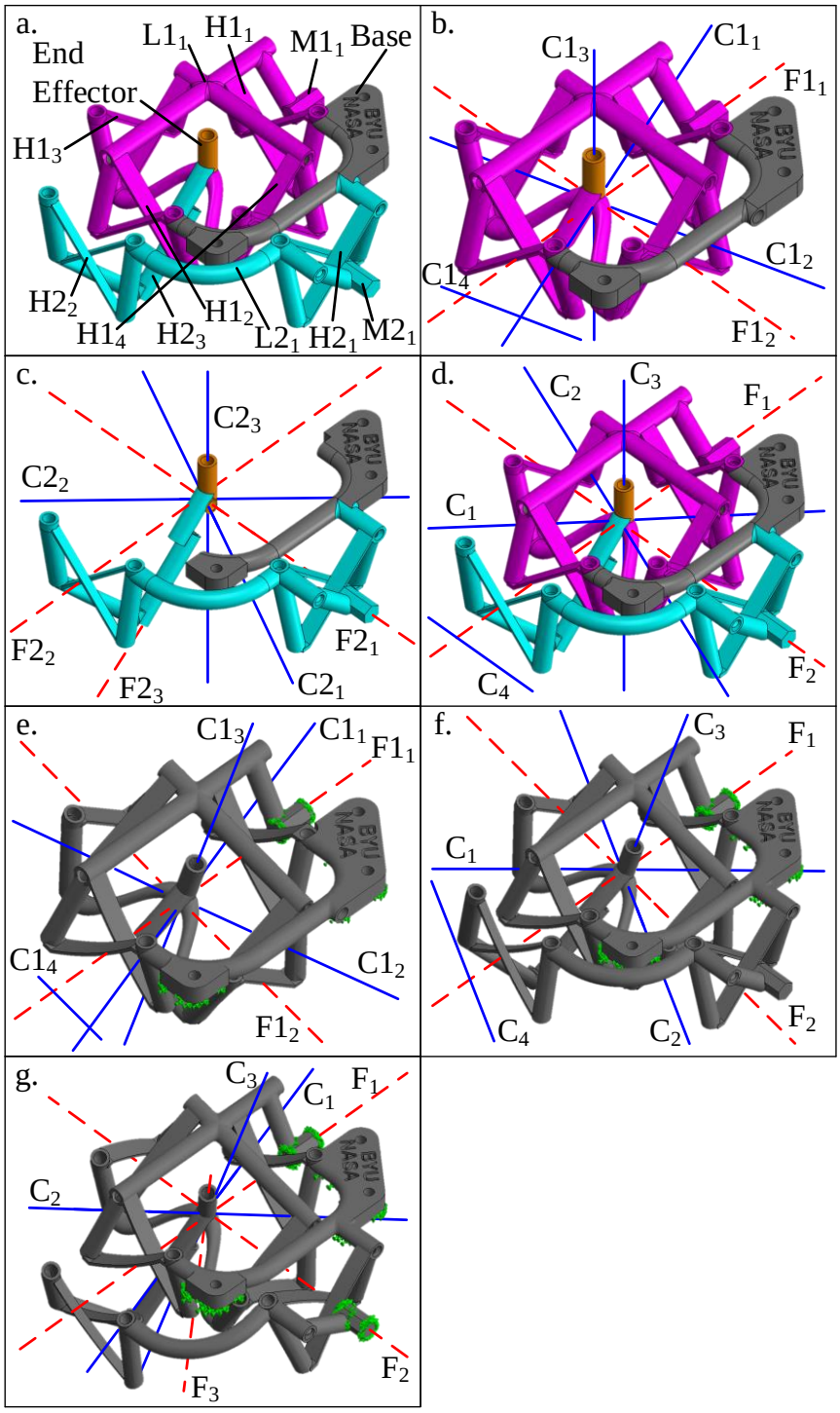

Fig. 12 BYU Space Pointing Mechanism: a. Full mechanism nominal configuration, b. First chain nominal configuration, c. Second chain nominal configuration, d. Full mechanism nominal configuration, e. First chain after rotation about $F1_1$, f. Full mechanism after single rotation about F_1, g. Full mechanism after both rotations

includes three constraint lines $C1_1$, $C1_2$, and $C1_3$ that are not all coplanar and intersect at the intersection of the two freedom lines. $C1_4$ is coplanar to both freedom lines but does not pass through their intersection.

The freedom and constraint spaces of the second chain in the nominal configuration are shown in in Fig. 12c. The flexural joints $H2_1$, $H2_2$, and $H2_3$ provide $F2_1$, $F2_2$, and $F2_3$, respectively. It should be noted that while the three freedom lines intersect at a single point, $F2_3$ does not lie in the same plane as the other two freedom lines. This intersection point is shared by the two DoFs from the first chain. $F2_1$ and $F2_2$ are also coplanar to both freedom lines and collinear to $F1_2$ and $F1_1$, respectively. The corresponding constraint space comprises three constraint lines, $C2_1$, $C2_2$, and $C2_3$, which are not all coplanar but share the same intersection point.

A look at relationships between the freedom lines of the two chains shows the intent behind the architecture of this mechanism. By connecting two chains that have collinear pitch and yaw DoFs, this mechanism serves as a parallel kinematic articulated wrist mechanism as reflected by the nominal constraint and freedom spaces shown in Fig. 12d. The mechanism's constraint space is the same as the first chain's because all three of the second chain's DoCs are redundant. Thus, the mechanism's freedom space in its nominal configuration is also identical to the first chain's. However, some of the important geometric relationships that make this possible no longer hold in displaced configurations.

The constraint and freedom spaces of the first chain after a single rotation about $F1_1$ are shown in Fig. 12e. $F1_2$ rotates along with the End Effector and the two freedom lines maintain the same point of intersection and their orthogonal relationship. The plane composed of the two freedom lines also remains orthogonal to the central axis. As expected, the constraint space of

the chain also rotates about $F1_1$ but maintains all of the same relationships as in the nominal configuration.

The constraint and freedom spaces for the overall mechanism after a single rotation about F_1 are shown in Fig. 12f. The second chain primarily allows this displacement through deformation of $H2_2$. Thus the freedom and constraint spaces of the second chain do not change significantly from the nominal configuration. As in the case of the nominal configuration, the mechanism's constraint and freedom spaces are dictated by the corresponding spaces of the first chain. Therefore, the mechanism appears to remain an articulated wrist mechanism. However, an important result of this rotation is that F_2 (dictated by $F1_2$) is no longer collinear to $F2_1$, which is still the axis of rotation of the actuator connected to the second chain. Given this, for the second actuation about $F2_1$ to happen, the flexural pivots $H1_3$ and $H1_4$ would need finite compliance about the two DoCs in each that do not pass through the intersection of $F1_1$ and $F2_1$; this compliance will require twisting along the flexural blades of each pivot. Similarly, $H2_2$ and $H2_3$ would also need to have finite compliance about the two DoCs that do not intersect $F1_1$ for a rotation about $F1_2$ to be possible. A similar issue occurs if the rotations take place in the opposite order and would require analogous compliances in the DoCs of the flexural pivots.

This analysis shows that if this mechanism were to be composed entirely of joints that are ideal (i.e. completely rigid in their DoCs), it would only be able to rotate along one of the two rotational DoFs at a time. However, this mechanism behaves as an articulated wrist mechanism where both pitch and yaw can be simultaneously actuated if pivots $H1_3$, $H1_4$, $H2_2$, and $H2_3$ have finite compliance along the DoCs specified above. This shows how intentional use of compliance can enable functionality that would otherwise not be possible. With the specified compliance in DoCs, the constraint and freedom spaces of this mechanism after rotations about $F1_1$ and $F2_1$ are

shown in Fig. 12g. The introduction of compliance brings an unintended and uncontrolled DoF F_3 but ensures that actuation is possible along $F1_1$ and $F2_1$ (represented by F_1 and F_2). Despite appearing to have the freedom space of a spherical joint, the stiffness about F_3 is significantly higher than about either of the other two DoFs.

While the nature and location of the pitch and yaw freedom lines do not appear to change due to mechanism kinematics, these lines may still drift due to small but finite deformations along DoCs of some of the flexural pivots. This can lead to these freedom lines not intersecting. However, these deviations should be relatively small compared to the size of the mechanism. The range of motion of this mechanism is tied to the amount of compliance incorporated in the specified DoCs of the flexural pivots. This compliance will also reduce load bearing and transmission capabilities because loading will cause increasing deformation of the flexural pivots in their DoCs. One instance of this mechanism [17], made monolithically out of titanium, provided a modest range of motion (~ 15° cone) with moderate to high stiffness expected in its DoCs. This was meant for a jet pointing application involving large loads but small ranges of motion. While not arranged for an open space around the intersection of its DoFs in the figure, it can be arranged to create this open space. With appropriate tuning of the stiffness of the flexural pivots, this mechanism could be used for applications that require a remote center such as those involving a human interface.

CHAPTER 3

Conclusion

The performance attributes of all eight mechanisms are summarized in Table 1. Of these, the nature and location of the two rotational DoFs in the nominal and displaced configurations are two key attributes that allow for a functional categorization of the mechanisms. Mechanisms that provide purely rotational pitch and yaw DoFs that do not translate over their workspace, such as the Dual Arch, Tip-Tilt Plate, and Agile Eye mechanisms, can be used in a wide range of applications that require tracing a constant radius spherical section. However, it is difficult to find or design a parallel kinematic articulated wrist mechanism belonging to this category that is also able to trace an entire hemisphere; mechanisms belonging to this category can typically achieve only a portion of a hemisphere limited by singularities and/or link collision. This is an important area of future investigation and innovation. Mechanisms in which the nature of the pitch and yaw DoFs change such as the OmniWrist and 3-Spherical Kinematic Chain Parallel mechanisms are limited to use in applications that either do not require a workspace with constant radius or can compensate for this nonideal behavior. Mechanisms in which the locations of the pitch and yaw DoFs can drift such as the FlexDex and BYU Space Pointing mechanisms are also similarly limited.

The FlexDex and BYU Space Pointing mechanisms also stand apart for their intentional use of compliance, which enables functionality that may be difficult to achieve using ideal links and joints. However, this approach also leads to tradeoffs, including potential drifting of the location of their rotational DoFs, as noted above. Location of DoFs for such mechanisms can be

both orientation-dependent and load-dependent because their links and joints may deform under loading. Compliance also impacts the mechanism's range of motion and load bearing and transmission capabilities.

Another important design strategy utilized by many of the mechanisms is overconstraint, which can be used for several reasons. One reason is to enable ground-mounted actuation for each DoF, as is the case for the Agile Eye and BYU Space Pointing mechanisms. Another reason is to increase the load bearing capabilities; this can be done for the OmniWrist and Tip-Tilt Plate mechanisms, in which additional serial chains can be added to improve stiffness. Load transmission capability can similarly be improved and can also enable the overactuation of DoFs (e.g. providing independent actuators to all four of the OmniWrist III's serial chains). In each of these scenarios, overconstraint is only possible when the additional constraint lines are redundant throughout the mechanism's range of motion. This condition can be met by introducing small clearances into joints or by utilizing compliance. For example, compliance is introduced in the FlexDex mechanism to ensure that constraint lines remain redundant. There are important tradeoffs with either approach, but they can contribute to important performance improvements.

Finally, it is important to note the diversity in mechanisms that can produce the same mechanism freedom space. For example, both the Dual Arch and FlexDex mechanisms share similar freedom spaces when the FlexDex mechanism's compliant strips are assumed compliant in torsion. The OmniWrist mechanisms also have similar freedom spaces because each of the OmniWrist III's serial chains provides a constraint space that is the same as the combined constraint space of the OmniWrist V's outer and central serial chains. Despite having similar freedom spaces, each mechanism provides a unique set of performance tradeoffs that makes it better suited for different applications.

Table 1 Performance Attributes of the Articulated Wrist Mechanisms

(N – Nominal Configuration, D – Displaced Configuration, R – with ideal links and joints, F – with some compliance)

Mechanism	Total Number of DoFs	Location of Pitch and Yaw DoFs	Nature of Pitch and Yaw DoFs	Load Bearing Capability	Load Transmission Capability
Dual Arch	4 (N, D)	On Central Axis (N, D)	Rotational (N, D)	High	High
Tip-Tilt Plate	2 (N, D)	On Central Axis (N, D)	Rotational (N, D)	High	High
Agile Eye	3 (N, D)	On Central Axis (N, D)	Rotational (N, D)	Moderate	Moderate
OmniWrist III	2 (N, D)	On Central Axis (N, D)	Rotational (N), Screw (D)	Moderate	Moderate
OmniWrist V	2 (N, D)	On Central Axis (N, D)	Rotational (N), Screw (D)	High	High
3-Spherical Kinematic Chain Parallel	3 (N, D)	On Central Axis (N, D)	Rotational (N), Screw (D)	Moderate	Moderate
FlexDex	3 (N), 2 (DR), 4 (DF)	On Central Axis (N), Can Drift (DF)	Rotational (N, D)	Low	Low
BYU Space Pointing	2 (N), 1 (DR), 3 (DF)	On Central Axis (N), Can Drift (DF)	Rotational (N, D)	Moderate	Moderate

BIBLIOGRAPHY

[1] Salerno, M., Zhang, K., Menciassi, A., and Dai, J. S., 2016, "A Novel 4-DOF Origami Grasper With an SMA-Actuation System for Minimally Invasive Surgery," *IEEE Transactions on Robotics*, **32**(3), pp. 484–498.

[2] Sakurai, H., Kanno, T., and Kawashima, K., 2016, "Thin-Diameter Chopsticks Robot for Laparoscopic Surgery," *2016 IEEE International onference on Robotics and Automation (ICRA)*, pp. 4122–4127.

[3] Shi, Z. Y., Liu, D., and Wang, T. M., 2014, "A Shape Memory Alloy-Actuated Surgical Instrument with Compact Volume," *International Journal of Medical Robotics and Computer Assisted Surgery*, **10**(4), pp. 474–481.

[4] Van Meer, F., Giraud, A., Esteve, D., and Dollat, X., 2005, "A Disposable Plastic Compact Wrist for Smart Minimally Invasive Surgical Tools," *2005 IEEE/RSJ International Conference on Intelligent Robots and Systems, IROS*.

[5] Navarro, J. S., Garcia, N., Perez, C., Fernandez, E., Saltaren, R., and Almonacid, M., 2010, "Kinematics of a Robotic 3UPS1S Spherical Wrist Designed for Laparoscopic Applications," *The International Journal of Medical Robotics and Computer Assisted Surgery*, **6**(3), pp. 291–300.

[6] Schoepp, H., 2013, "Axial Surgical Trajectory Guide," US 2013/0066334 A1.

[7] Vischer, P., and Clavel, R., 2000, "Argos: A Novel 3-DoF Parallel Wrist Mechanism," *International Journal of Robotics Research*, **19**(1), pp. 5–11.

[8] Kuo, C.-H., and Dai, J. S., 2009, "Robotics for Minimally Invasive Surgery: A Historical Review from the Perspective of Kinematics," *International Symposium on History of Machines and Mechanisms*, pp. 337–354.

[9] Awtar, S., Trutna, T. T., Nielsen, J. M., Abani, R., and Geiger, J., 2010, "FlexDex™: A

Minimally Invasive Surgical Tool with Enhanced Dexterity and Intuitive Control," *ASME Journal of Medical Devices*, **4**(3), pp. 1–8.

[10] Awtar, S., and Nielsen, J., 2019, "Parallel Kinematic Mechanisms with Decoupled Rotational Motions," US 10,405,936 B2.

[11] Beurrier, H. R., 1968, "Output Control Device with Adjustable Self-Returning Null," US 3,394,611.

[12] Shimomura, H., 2000, "Multi-Direction Input Device," US 6,078,247.

[13] Rosheim, M. E., 1989, *Robot Wrist Actuators*, Wiley, NY.

[14] Rosheim, M. E., 1994, *Robot Evolution: The Development of Anthrobotics*, Wiley, NY.

[15] Gosselin, C. M., St. Pierre, E., and Gagné, M., 1996, "On the Development of the Agile Eye," *IEEE Robotics & Automation Magazine*, **3**(4), pp. 29–37.

[16] Rosheim, M. E., and Sauter, G. F., 2002, "New High-Angulation Omni-Directional Sensor Mount," *Proceedings of SPIE, Free-Space Laser Communication and Laser Imaging II*, **4821**, pp. 163-174.

[17] Merriam, E. G., Jones, J. E., Magleby, S. P., and Howell, L. L., 2013, "Monolithic 2 DOF Fully Compliant Space Pointing Mechanism," *Mechanical Sciences*, **4**(2), pp. 381–390.

[18] Hopkins, J. B., Panas, R. M., Song, Y., and White, C. D., 2017, "A High-Speed Large-Range Tip-Tilt-Piston Micromirror Array," *Journal of Microelectromechanical Systems*, **26**(1), pp. 196–205.

[19] McNamara, I. E., Toombs, N. J., Kim, J., Mcnamara, D. P., and Rapp, N. L., 2019, "Autonomous Fire Locating And Suppression Apparatus And Method", US 2019/0054333 A1.

[20] Hammond, F. L., Howe, R. D., and Wood, R. J., 2013, "Dexterous High-Precision

Robotic Wrist for Micromanipulation," *2013 16th International Conference on Advanced Robotics*.

[21] Awtar, S., Bernard, C., Boklund, N., Master, A., Ueda, D., and Craig, K., 2002, "Mechatronic Design of a Ball-on-Plate Balancing System," *Mechatronics*, **12**(2), pp. 217–228.

[22] Liu, G., Gao, J., Yue, H., Zhang, X., and Lu, G., 2006, "Design and Kinematics Simulation of Parallel Robots for Ankle Rehabilitation," *2006 IEEE International Conference on Mechatronics and Automation*, pp. 1109–1113.

[23] Dai, J. S., Zhao, T., and Nester, C., 2004, "Sprained Ankle Physiotherapy Based Mechanism Synthesis and Stiffness Analysis of a Robotic Rehabilitation Device," *Autonomous Robots*, **16**, pp. 207–218.

[24] Saglia, J. A., Dai, J. S., and Caldwell, D. G., 2008, "Geometry and Kinematic Analysis of a Redundantly Actuated Parallel Mechanism That Eliminates Singularities and Improves Dexterity," *ASME Journal of Mechanical Design* , **130**, pp. 124501-1-124501-5.

[25] Blanding, D. L., 1999, *Exact Constraint: Machine Design Using Kinematic Principles*, ASME Press, NY.

[26] Hunt, K. H., 1979, *Kinematic Geometry of Mechanisms*, Oxford University Press, USA.

[27] Huang, Z., and Li, Q. C., 2002, "General Methodology for Type Synthesis of Symmetrical Lower-Mobility Parallel Manipulators and Several Novel Manipulators," Int. J. Rob. Res., **21**(2), pp. 131–145.

[28] Zhao, J. S., Zhou, K., and Feng, Z. J., 2004, "A Theory of Degrees of Freedom for Mechanisms," Mech. Mach. Theory, **39**(6), pp. 621–643.

[29] Dai, J. S., Huang, Z., and Lipkin, H., 2006, "Mobility of Overconstrained Parallel

Mechanisms," *ASME Journal of Mechanical Design*, **128**(1), pp. 220–229.

[30] Huang, Z., Liu, J., and Li, Q., 2008, "A Unified Methodology for Mobility Analysis Based on Screw Theory," *Smart Devices and Machines for Advanced Manufacturing*, Springer-Verlag, London, pp. 49–78.

[31] Zhao, J., Feng, Z., Chu, F., and Ma, N., 2014, *Advanced Theory of Constraint and Motion Analysis for Robot Mechanisms*, Elsevier Inc.

[32] McCarthy, J. M., and Soh, G. S., 2011, *Geometric Design of Linkages*, Springer.

[33] Hopkins, J. B., 2010, *Design of Flexure-Based Motion Stages for Mechatronic Systems via Freedom, Actuation and Constraint Topologies (FACT)*, Massachusetts Institute of Technology.

[34] Hopkins, J. B., and Culpepper, M. L., 2010, "Synthesis of Multi-Degree of Freedom, Parallel Flexure System Concepts via Freedom and Constraint Topology (FACT) - Part I: Principles," *Precision Engineering*, **34**(2), pp. 259–270.

[35] Hopkins, J. B., and Culpepper, M. L., 2010, "Synthesis of Multi-Degree of Freedom, Parallel Flexure System Concepts via Freedom and Constraint Topology (FACT). Part II: Practice," *Precision Engineering*, **34**(2), pp. 271–278.

[36] Kong, X., and Gosselin, C. M., 2004, "Type Synthesis of 3-DOF Spherical Parallel Manipulators Based on Screw Theory," *ASME Journal of Mechanical Design*, **126**(1), pp. 101–108.

[37] Su, H. J., Dietmaier, P., and McCarthy, J. M., 2003, "Trajectory Planning for Constrained Parallel Manipulators," *ASME Journal of Mechanical Design*, **125**(4), pp. 709–716.

[38] Zhang, K., Fang, Y., Fang, H., and Dai, J. S., 2010, "Geometry and Constraint Analysis of the Three-Spherical Kinematic Chain Based Parallel Mechanism," *ASME Journal of*

Mechanisms and Robotics, **2**(3).

[39] Gosselin, C., and Angeles, J., 1990, "Singularity Analysis of Closed-Loop Kinematic Chains," *IEEE Transactions on Robotics and Automation*, **6**(3), pp. 281–290.

[40] Bohigas, O., Manubens, M., Ros, L., and Manubens, M., 2017, *Singularities of Robot Mechanisms*, Springer International Publishing Switzerland.

[41] Rosheim, M. E., 2003, "Robotic Manipulator," US 6,658,962 B1.

[42] Rosheim, M. E., 2017, "Robot Manipulator with Spherical Joints," US 9,630,326 B2.

[43] "Singularities of a 3RRR Mechanism - YouTube" https://www.youtube.com/watch?v=xV3m6ioilnc.

[44] Bonev, I. A., Chablat, D., and Wenger, P., 2006, "Working and Assembly Modes of the Agile Eye," *Proceedings - IEEE International Conference on Robotics and Automation*, pp. 2317–2322.

[45] Asada, K., and Granito, J. A. C., 1985, "Kinematic and Static Characterization of Wrist Joints Their Optimal Design," *1985 IEEE International Conference on Robotics and Automation*, pp. 244–250.

[46] Gosselin, C., and Angeles, J., 1989, "The Optimum Kinematic Design of a Spherical Three-Degree-of-Freedom Parallel Manipulator," *ASME Journal of Mechanical Design*, **111**(2), pp. 202–207.

[47] Tao, Z., and An, Q., 2013, "Interference Analysis and Workspace Optimization of 3-RRR Spherical Parallel Mechanism," *Mechanism and Machine Theory*, **69**, pp. 62–72.